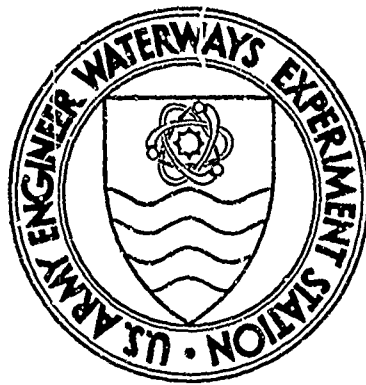


AD735343



MISCELLANEOUS PAPER S-7I-13

SOME THEORETICAL AND EXPERIMENTAL IMPLICATIONS OF CONSTANT SHEAR MODULUS CONSTITUTIVE MODELS

by

B. Rohani, J. G. Jackson, Jr.



Reproduced by
NATIONAL TECHNICAL
INFORMATION SERVICE
Springfield, Va. 22151
December 1971

DDC
DRAFTED JAN 17 1972
RELEASING C

Sponsored by Defense Nuclear Agency

Conducted by U. S. Army Engineer Waterways Experiment Station, Vicksburg, Mississippi

APPROVED FOR PUBLIC RELEASE; DISTRIBUTION UNLIMITED

54

DISCLAIMER NOTICE

**THIS DOCUMENT IS BEST QUALITY
PRACTICABLE. THE COPY FURNISHED
TO DTIC CONTAINED A SIGNIFICANT
NUMBER OF PAGES WHICH DO NOT
REPRODUCE LEGIBLY.**

Unclassified
Security Classification

DOCUMENT CONTROL DATA - R & D

(Security classification of title, body of abstract and indexing annotation must be entered when the overall report is classified)

1. ORIGINATING ACTIVITY (Corporate author) U. S. Army Engineer Waterways Experiment Station, Vicksburg, Mississippi		2a. REPORT SECURITY CLASSIFICATION Unclassified
2b. GROUP		
3. REPORT TITLE SOME THEORETICAL AND EXPERIMENTAL IMPLICATIONS OF CONSTANT SHEAR MODULUS CONSTITUTIVE MODELS		
4. DESCRIPTIVE NOTES (Type of report and inclusive dates) Final report		
5. AUTHOR(S) (First name, middle initial, last name) Behzad Rohani, John G. Jackson, Jr.		
6. REPORT DATE December 1971	7a. TOTAL NO. OF PAGES 57	7b. NO. OF REFS 4
8. CONTRACT OR GRANT NO.		
9. PROJECT NO. NWER Subtask SB209 Miscellaneous Paper S-71-13		
10. DISTRIBUTION STATEMENT Approved for public release; distribution unlimited.		
11. SUPPLEMENTARY NOTES	12. SPONSORING MILITARY ACTIVITY Defense Nuclear Agency Washington, D. C.	
13. ABSTRACT Some of the theoretical and experimental implications of isotropic incremental elastic-plastic constitutive models formulated with constant values for the shear modulus G are examined. Two types of constant G models are considered, i.e. a single constant value of G for loading and unloading and two separate values of G , one for loading and one for unloading. These material property specifications are successively coupled with four increasingly more realistic idealized stress-strain relations representing constrained modulus M functions obtained for a state of uniaxial strain and a von Mises-type limiting shear envelope characteristic of that specified for the classical Prandtl-Reuss material. The resulting models are used to calculate mean normal stress or pressure versus volumetric strain and uniaxial strain principal stress difference versus pressure relations for qualitative comparison with observed test phenomena. The results from this simple examination of several highly idealized material descriptions indicate that many of the behavior characteristics of real earth materials often recorded during laboratory tests can be simulated, at least qualitatively, by elastic-plastic constitutive models of the constant G type by observing certain restrictions on the material property parameters G and M . Other characteristic phenomena, however, cannot be mirrored with these types of models under any circumstances. The constitutive equations of a classical Prandtl-Reuss material and the behavior of this ideal model for conditions of uniaxial strain are included in an appendix for reference and informational purposes.		

DD FORM 1473
REV. 1 JAN 68

REPLACES DD FORM 1473, 1 JAN 68, WHICH IS
OBSOLETE FOR ARMY USE.

Destroy this report when no longer needed. Do not return
it to the originator.

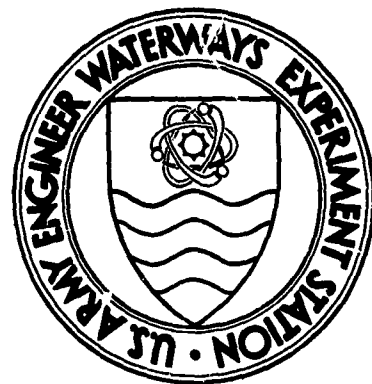
The findings in this report are not to be construed as an official
Department of the Army position unless so designated
by other authorized documents.

APPROVED FOR	
WHITE SECTION	<input checked="" type="checkbox"/>
BUFF SECTION	<input type="checkbox"/>
DRAFTED	
JUSTIFICATION	
BY	
DISTRIBUTION/AVAILABILITY COPIES	
DISP.	AVAIL. DAS/OF SPECIAL
A	

Unclassified

Security Classification

14. KEY WORDS	LINK A		LINK B		LINK C	
	ROLE	WT	ROLE	WT	ROLE	WT
Constitutive models						
Shear modulus						
Stress-strain relations						



MISCELLANEOUS PAPER S-71-13

SOME THEORETICAL AND EXPERIMENTAL IMPLICATIONS OF CONSTANT SHEAR MODULUS CONSTITUTIVE MODELS

by

B. Rohani, J. G. Jackson, Jr.



December 1971

Sponsored by Defense Nuclear Agency
NWER Subtask SB209

Conducted by U. S. Army Engineer Waterways Experiment Station, Vicksburg, Mississippi

ARMY-MRC VICKSBURG, MISS

APPROVED FOR PUBLIC RELEASE; DISTRIBUTION UNLIMITED

ABSTRACT

Some of the theoretical and experimental implications of isotropic incremental elastic-plastic constitutive models formulated with constant values for the shear modulus G are examined. Two types of constant G models are considered, i.e. a single constant value of G for loading and unloading and two separate values of G , one for loading and one for unloading. These material property specifications are successively coupled with four increasingly more realistic idealized stress-strain relations representing constrained modulus M functions obtained for a state of uniaxial strain and a von Mises-type limiting shear envelope characteristic of that specified for the classical Prandtl-Reuss material. The resulting models are used to calculate mean normal stress or pressure versus volumetric strain and uniaxial strain principal stress difference versus pressure relations for qualitative comparison with observed test phenomena.

The results from this simple examination of several highly idealized material descriptions indicate that many of the behavior characteristics of real earth materials often recorded during laboratory tests can be simulated, at least qualitatively, by elastic-plastic constitutive models of the constant G type by observing certain restrictions on the material property parameters G and M . Other characteristic phenomena, however, cannot be mirrored with these types of models under any circumstances.

The constitutive equations of a classical Prandtl-Reuss material and the behavior of this ideal model for conditions of uniaxial strain are included in an appendix for reference and informational purposes.

Preceding page blank

PREFACE

The work described herein is part of a continuing research effort being conducted by personnel of the Soils Division, U. S. Army Engineer Waterways Experiment Station (WES), aimed at developing physically realistic and theoretically satisfying constitutive models for a broad range of soil and rock materials for use as input to free-field ground shock calculation computer codes. This particular study, which deals in general terms with relatively simple idealizations of material behavior, developed as an adjunct to an investigation begun by CPT J. A. Spitznagel, CE, into the use of constant shear modulus-type constitutive models to represent the actual behavior observed in the WES Soil Dynamics Laboratory during numerous tests on soils and weak sedimentary rocks. The theoretical analyses of these idealized models were performed during the period February-April 1971 by Dr. Behzad Rohani; this paper was written by Dr. Rohani and Dr. J. G. Jackson, Jr.

The project is sponsored by the Defense Nuclear Agency as part of their Nuclear Weapons Effects Research Subtask SB209, "Propagation of Ground Shock Through Earth Media." The work is being performed under the general direction of Messrs. J. P. Sale, R. G. Ahlvin, and R. W. Cunny, of the Soils Division, WES. The Director of WES during the preparation and publication of this report was COL Ernest D. Peixotto, CE. Technical Director was Mr. Fred R. Brown.

CONTENTS

ABSTRACT-----	3
PREFACE-----	4
CHAPTER 1 INTRODUCTION-----	7
1.1 Background-----	7
1.2 Purpose and Scope-----	9
CHAPTER 2 CONSTANT SHEAR MODULUS CONSTITUTIVE MODELS FOR STRESS STATES BELOW YIELD-----	13
2.1 Linear Elastic G Model for Materials with a Linear Elastic M -----	15
2.2 Linear Hysteretic G Model for Materials with a Linear Elastic M -----	16
2.3 Linear Elastic G Model for Materials with a Linear Hysteretic M -----	17
2.4 Linear Hysteretic G Model for Materials with a Linear Hysteretic M -----	19
2.5 Linear Elastic G Model for Materials with a Nonlinear Hysteretic M -----	20
2.6 Linear Hysteretic G Model for Materials with a Nonlinear Hysteretic M -----	20
CHAPTER 3 CONSTANT SHEAR MODULUS CONSTITUTIVE MODELS FOR STRESS STATES REACHING YIELD-----	28
3.1 Linear Elastic G Model for Materials with a Bilinear Hysteretic M -----	28
3.2 Linear Elastic G Model for Materials with a Nonlinear Hysteretic M -----	31
CHAPTER 4 CONCLUSIONS AND RECOMMENDATIONS-----	35
4.1 Conclusions-----	35
4.2 Recommendations-----	36
APPENDIX A CONSTITUTIVE EQUATIONS AND UNIAXIAL STRAIN BEHAVIOR FOR A PRANDTL-REUSS MATERIAL-----	39
A.1 Purpose-----	39
A.2 Constitutive Equations-----	39
A.2.1 Yield Criterion-----	39
A.2.2 Stress-Strain Relationship-----	40
A.3 Behavior Under Conditions of Uniaxial Strain-----	42
REFERENCES-----	50
FIGURES	
1.1 Principal stress difference versus principal strain differ- ence relations for linear elastic and linear hysteretic G models-----	11

1.2	Vertical stress versus vertical strain curves for conditions of uniaxial strain-----	12
2.1	Behavior of linear elastic material under conditions of uniaxial strain-----	22
2.2	Behavior of linear hysteretic shear modulus model for materials with a linear elastic constrained modulus under conditions of uniaxial strain-----	23
2.3	Behavior of linear elastic shear modulus model for materials with a linear hysteretic constrained modulus under conditions of uniaxial strain-----	24
2.4	Behavior of linear hysteretic shear modulus model for materials with a linear hysteretic constrained modulus under conditions of uniaxial strain-----	25
2.5	Behavior of linear elastic shear modulus model for materials with a nonlinear hysteretic constrained modulus under conditions of uniaxial strain-----	26
2.6	Behavior of linear hysteretic shear modulus model for materials with a nonlinear hysteretic constrained modulus under conditions of uniaxial strain-----	27
3.1	Behavior of linear elastic shear modulus model for elastic-plastic materials with a bilinear hysteretic constrained modulus under conditions of uniaxial strain-----	33
3.2	Behavior of linear elastic shear modulus model for elastic-plastic materials with a nonlinear hysteretic constrained modulus under conditions of uniaxial strain-----	34
A.1	von Mises yield surface in principal stress space-----	47
A.2	Uniaxial strain configuration in cylindrical coordinate-----	48
A.3	Behavior of Prandtl-Reuss material under conditions of uniaxial strain-----	49

CHAPTER 1

INTRODUCTION

1.1 BACKGROUND

The constitutive equations currently used to represent various types of earth media in two-dimensional ground shock calculation codes are based on the assumption of isotropic incremental elastic-plastic material behavior. In the elastic range, material behavior is described by the following incremental constitutive relation that effectively separates the deformation into hydrostatic and deviatoric components.¹

$$\dot{\sigma}_{ij} = K \dot{\epsilon}_{kk} \delta_{ij} + 2G(\dot{\epsilon}_{ij} - \frac{1}{3} \dot{\epsilon}_{kk} \delta_{ij}) \quad (1.1)$$

where $\dot{\sigma}_{ij}$ = components of the total stress increment tensor

$$= \frac{1}{3} \dot{\sigma}_{kk} \delta_{ij} + \dot{s}_{ij}$$

$$K = \text{bulk modulus} = \frac{p}{\dot{\epsilon}_{kk}}$$

$\dot{\epsilon}_{kk}$ = sum of the incremental normal strains = incremental change in volumetric strain

δ_{ij} = Kronecker delta

$$G = \text{shear modulus} = \frac{1}{2} \frac{\dot{s}_{ij}}{\dot{\epsilon}_{ij}}$$

$\dot{\epsilon}_{ij}$ = components of the total strain increment tensor

$$= \frac{1}{3} \dot{\epsilon}_{kk} \delta_{ij} + \dot{\epsilon}_{ij}$$

$\dot{\sigma}_{kk}$ = sum of the incremental normal stresses = $3p$

\dot{s}_{ij} = components of the incremental stress deviator tensor

$\dot{\epsilon}_{ij}$ = components of the incremental strain deviator tensor

¹ Elastic range as used in this paper does not imply linear reversible behavior of the material, but rather refers to all stress-strain responses for deviatoric stress states less than that defined by an explicit plastic yield function.

Nonlinear behavior is incorporated by making K and G functions of stress and/or strain invariants. Hysteretic behavior is taken into account by using different values of K and G on loading and unloading. A pseudoplastic behavior is thus built into the incremental constitutive relation (Equation 1.1) in the form of permanent compaction prior to yield.

Classical plasticity is incorporated into the model by specifying a yield condition that effectively serves to limit the maximum shear strength of the material. The yield surface is usually a combination of the Prager-Drucker and von Mises types, often with a functional form that ensures a smooth transition from the former to the latter with increasing pressure (References 1 and 2).

With zero work hardening, the yield function is specified by a relation of the form

$$\sqrt{(J'_2)_{\max}} = f(p) \quad (1.2)$$

where J'_2 = second invariant of the stress deviator tensor = $\frac{1}{2} s_{ij} s_{ij}$

p = mean normal stress or pressure = $\frac{1}{3} \sigma_{kk}$

s_{ij} = components of the stress deviator tensor

From within this generalized description of elastic-plastic material behavior, many specific descriptions are available, depending upon the various restrictions placed on the constitutive property parameters K , G , and $\sqrt{(J'_2)_{\max}}$. One of the more common versions involves considerable flexibility in describing volume change characteristics by permitting K to be defined by nonlinear polynomial functions while restricting the description of shear behavior to constant values for G and $\sqrt{(J'_2)_{\max}}$. The significance of such restrictions can perhaps best be illustrated by examining the behavior of these constant shear modulus models when subjected to the states of stress most often employed in the laboratory to experimentally determine the stress-strain response of actual earth materials.

The testing technique most frequently used for studying stress-strain

response in the laboratory in conjunction with ground shock problems involves confining undisturbed specimens so that they deform in an undrained state of uniaxial strain under an applied transient stress (Reference 3). The test results are usually illustrated through a plot of vertical stress versus vertical strain; the slopes of such plots define the constrained modulus M , i.e.²

$$M = \left(\frac{\dot{\sigma}_z}{\dot{\epsilon}_z} \right)_{\text{uniaxial strain}} = K + \frac{4}{3} G \quad (1.3)$$

Triaxial shear tests are normally used to determine relationships between $\sqrt{J_2' \max}$ or maximum principal stress difference $(\sigma_z - \sigma_r)_{\max}$ and p . For a given material, a unique path of $(\sigma_z - \sigma_r)$ versus p is also described by a material undergoing uniaxial strain loading and unloading; the slopes along a stress path of this type define the ratio of shear modulus to bulk modulus, i.e.

$$\left(\frac{\dot{\sigma}_z - \dot{\sigma}_r}{\dot{p}} \right)_{\text{uniaxial strain}} = \frac{2G}{K} \quad (1.4)$$

Thus, as an aid in understanding the practical significance of constant G constitutive models, it is helpful to examine, for a given uniaxial strain σ_z versus ϵ_z relation and a given triaxial shear envelope, the characteristic features of the corresponding p versus ϵ_{kk} and uniaxial strain $(\sigma_z - \sigma_r)$ versus p relationships imposed by the further specification of a constant value for G .

1.2 PURPOSE AND SCOPE

The purpose of this paper is to examine some of the theoretical and

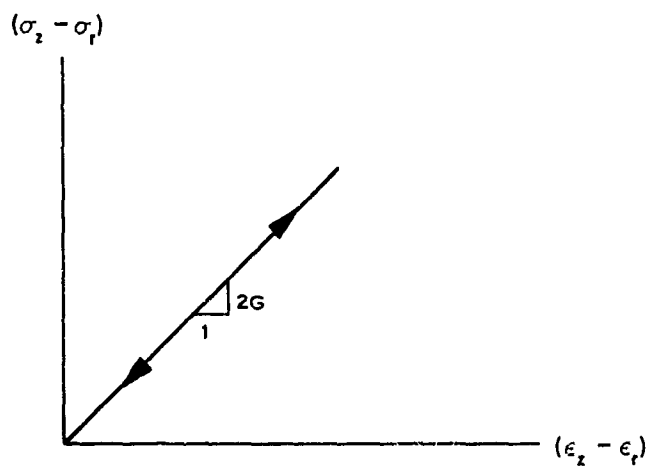
² The laboratory tests currently used for soil property investigations are axially symmetric so that the specimens can be analyzed in terms of coordinates z and r denoting vertical and radial directions, respectively.

experimental implications of isotropic incremental elastic-plastic constitutive models formulated with constant values for the shear modulus G . Two types of constant shear modulus models will be considered. The first model, in which one single constant value of G is used for loading and unloading, is referred to as a "linear elastic G model." The second, in which two separate constant values of G are specified, one for loading and one for unloading, is called the "linear hysteretic G model." Shear stress-shear strain diagrams for both models are given in Figure 1.1.

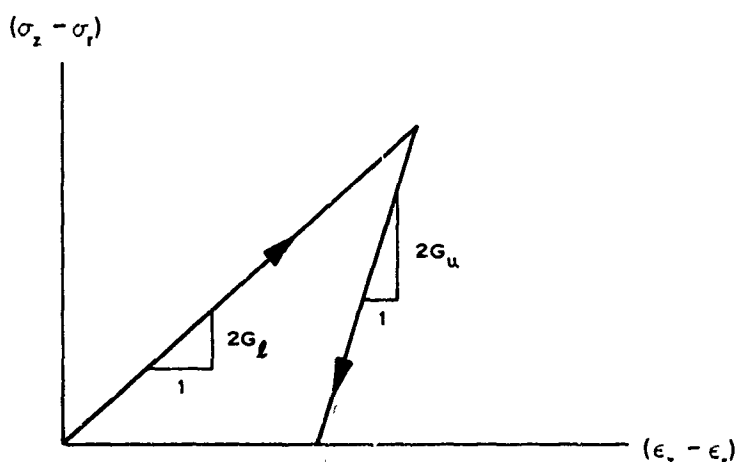
Four idealized uniaxial strain ϵ_z versus σ_z relations are used in conjunction with the two constant G relations. The first represents the simplest idealization, i.e. that defined by a linear elastic constrained modulus. The second is in the linear hysteretic form defined by separate constant values for M , i.e. one for loading and one for unloading. The third represents a bilinear hysteretic constrained modulus description and the fourth a general nonlinear hysteretic description. The four relations are diagramed in Figure 1.2.

It is assumed that plastic behavior is governed by a von Mises-type yield criterion as postulated for the classical Prandtl-Reuss material. Chapter 2 presents an analysis of six models, developed by successively coupling the two constant G descriptions (Figure 1.1) with the M descriptions outlined in Figures 1.2a, b, and d, subjected to maximum deviatoric stress levels insufficient to invoke the yield criterion. Two cases in which the deviatoric stress paths reach the plastic yield surface are examined in Chapter 3; these cases are defined by successively coupling the linear elastic constant G descriptions with the two M descriptions given in Figures 1.2c and d.

For reference and informational purposes, the mathematical constitutive equations for a linear elastic-plastic model of an ideal Prandtl-Reuss material are presented and its uniaxial strain behavior is examined in Appendix A.

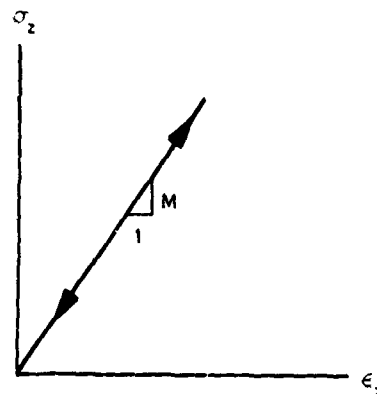


a. LINEAR ELASTIC G

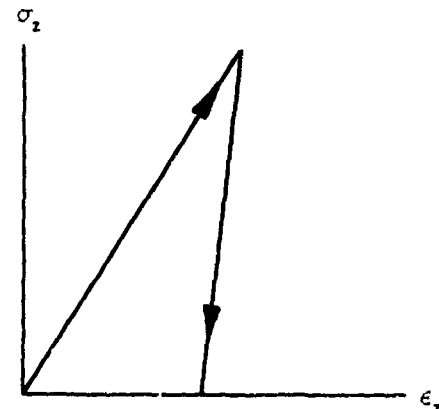


b. LINEAR HYSTERETIC G

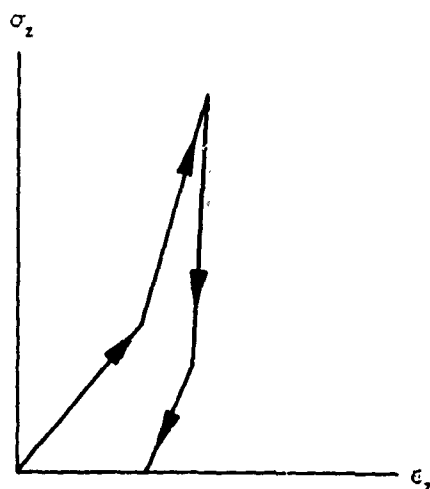
Figure 1.1 Principal stress difference versus principal strain difference relations for linear elastic and linear hysteretic G models.



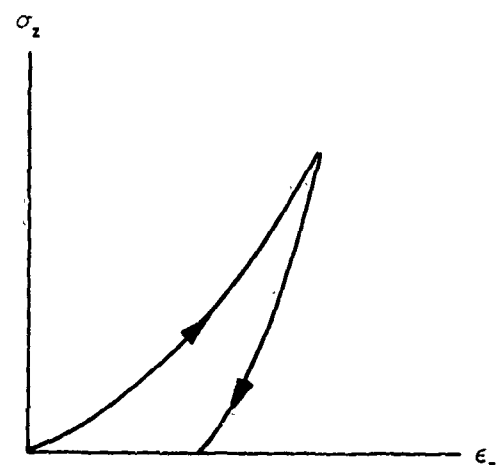
a. LINEAR ELASTIC M



b. LINEAR HYSTERETIC M



c. BILINEAR HYSTERETIC M



d. NONLINEAR HYSTERETIC M

Figure 1.2 Vertical stress versus vertical strain curves for conditions of uniaxial strain.

CHAPTER 2

CONSTANT SHEAR MODULUS CONSTITUTIVE MODELS FOR STRESS STATES BELOW YIELD

The basic constitutive relationship in the elastic range is Equation 1.1, which contains two material constants (or functions) K and G . Equation 1.1 can also be written in terms of constrained modulus M and shear modulus G by utilizing Equation 1.3, i.e.

$$\dot{\sigma}_{ij} = M \dot{\epsilon}_{kk} \delta_{ij} + 2G(\dot{\epsilon}_{ij} - \dot{\epsilon}_{kk} \delta_{ij}) \quad (2.1)$$

The procedure adopted in this chapter to study the behavior of the two constant G models for subyield stress states (elastic range) is to assume that M and G are known for each model and then substitute in Equation 2.1 to calculate the pressure-volumetric strain or K relation and the uniaxial strain path of principal stress difference versus pressure. The calculated behavior is then discussed in terms of the general behavior observed during tests on actual earth materials.

If M_ℓ and G_ℓ denote the constrained and shear moduli, respectively, for virgin loading and M_u and G_u denote the corresponding values for unloading, the expressions for the pressure-volumetric strain relation and the stress path associated with the uniaxial strain test become

$$\text{Virgin loading} \left\{ \begin{array}{l} \dot{p} = \left(M_\ell - \frac{4}{3} G_\ell \right) \dot{\epsilon}_z = K_\ell \dot{\epsilon}_z \\ (\dot{\sigma}_z - \dot{\sigma}_r) = \left(\frac{2G_\ell}{M_\ell - \frac{4}{3} G_\ell} \right) \dot{p} = \frac{2G_\ell}{K_\ell} \dot{p} \end{array} \right. \quad (2.2a)$$

$$\left. \begin{array}{l} \dot{p} = \left(M_u - \frac{4}{3} G_u \right) \dot{\epsilon}_z = K_u \dot{\epsilon}_z \\ (\dot{\sigma}_z - \dot{\sigma}_r) = \left(\frac{2G_u}{M_u - \frac{4}{3} G_u} \right) \dot{p} = \frac{2G_u}{K_u} \dot{p} \end{array} \right. \quad (2.2b)$$

$$\text{Unloading and reloading} \left\{ \begin{array}{l} \dot{p} = \left(M_u - \frac{4}{3} G_u \right) \dot{\epsilon}_z = K_u \dot{\epsilon}_z \\ (\dot{\sigma}_z - \dot{\sigma}_r) = \left(\frac{2G_u}{M_u - \frac{4}{3} G_u} \right) \dot{p} = \frac{2G_u}{K_u} \dot{p} \end{array} \right. \quad (2.2c)$$

$$\left. \begin{array}{l} \dot{p} = \left(M_u - \frac{4}{3} G_u \right) \dot{\epsilon}_z = K_u \dot{\epsilon}_z \\ (\dot{\sigma}_z - \dot{\sigma}_r) = \left(\frac{2G_u}{M_u - \frac{4}{3} G_u} \right) \dot{p} = \frac{2G_u}{K_u} \dot{p} \end{array} \right. \quad (2.2d)$$

The values of loading and unloading shear moduli are constant throughout the calculations, whereas the values of loading and unloading constrained moduli could vary with stress level, in which case the construction of the model must be carried out incrementally by solving for compatible values of $(\dot{\sigma}_z - \dot{\sigma}_r)$ and \dot{p} corresponding to each pair of $\dot{\sigma}_z, \dot{\epsilon}_z$ values. The pertinent incremental relations are

$$(\dot{\sigma}_z - \dot{\sigma}_r) = 2G_s \dot{\epsilon}_z \quad \text{for loading} \quad (2.3a)$$

$$(\dot{\sigma}_z - \dot{\sigma}_r) = 2G_u \dot{\epsilon}_z \quad \text{for unloading-reloading} \quad (2.3b)$$

$$\dot{p} = \dot{\sigma}_z - \frac{2}{3} (\dot{\sigma}_z - \dot{\sigma}_r) \quad (2.3c)$$

The total quantities needed for plotting pertinent stress-strain and stress path relations are then obtained from the following expressions:

$$(\sigma_z)_i = (\sigma_z)_{i-1} + \dot{\sigma}_z \quad (2.4a)$$

$$(\epsilon_z)_i = (\epsilon_z)_{i-1} + \dot{\epsilon}_z \quad (2.4b)$$

$$(\sigma_z - \sigma_r)_i = (\sigma_z - \sigma_r)_{i-1} + (\dot{\sigma}_z - \dot{\sigma}_r) \quad (2.4c)$$

$$(p)_i = (p)_{i-1} + \dot{p} \quad (2.4d)$$

where $i = 1, \dots, m$. The calculation is performed in each increment of loading or unloading as if the material were elastic.

Six different models are considered in this chapter using various combinations of constrained and shear moduli as outlined in Section 1.2. The models are presented below in the order of increasing complexity.

2.1 LINEAR ELASTIC G MODEL FOR MATERIALS WITH A LINEAR ELASTIC M

This model corresponds to a linear elastic material and is obviously the simplest possible constitutive model available. It is presented here only to demonstrate the methodology used in this chapter. Since both the shear modulus and the constrained modulus are elastic, it implies that $M_u = M_l = M$ and $G_u = G_l = G$ so that the pressure-volumetric strain relation and the stress path associated with a state of uniaxial strain for this model become

$$p = \left(M - \frac{4}{3} G \right) \epsilon_z \quad (2.5a)$$

$$(\sigma_z - \sigma_r) = \left(\frac{2G}{M - \frac{4}{3} G} \right) p \quad (2.5b)$$

From thermodynamic considerations, it is necessary to impose the following inequalities on the shear modulus G and on Poisson's ratio ν

$$G > 0 \quad (2.6a)$$

$$-1 < \nu < \frac{1}{2} \quad (2.6b)$$

in order to insure the positive definite character of the quadratic form of the elastic strain energy function (Reference 4). Negative values of ν , however, have not been found experimentally for any isotropic elastic material. Thus, from purely phenomenological considerations, the restriction on ν should be revised to limit it to positive values, i.e.

$$0 < \nu < \frac{1}{2} \quad (2.7)$$

The relationship between ν , M , and G is given from elastic theory as

$$\nu = \frac{M - 2G}{2(M - G)} \quad (2.8)$$

The pertinent stress-strain and stress path plots for this simple elastic model are shown schematically in Figure 2.1.

2.2 LINEAR HYSTERETIC G MODEL FOR MATERIALS WITH A LINEAR ELASTIC M

Figures 2.2a and b depict the vertical stress-strain and the principal stress difference-strain difference relations, respectively, for this model under uniaxial strain conditions. Since the constrained modulus is linear elastic ($M_\ell = M_u = M$) and the shear modulus is linear hysteretic ($G_u > G_\ell$), the pressure-volumetric strain and the principal stress difference-pressure relations for the model are

$$\text{Virgin loading} \quad \left\{ \begin{array}{l} \dot{p} = \left(M - \frac{4}{3} G_\ell \right) \dot{\epsilon}_z \\ (\dot{\sigma}_z - \dot{\sigma}_r) = \left(\frac{2G_\ell}{M - \frac{4}{3} G_\ell} \right) \dot{p} \end{array} \right. \quad (2.9a)$$

$$\text{Unloading and reloading} \quad \left\{ \begin{array}{l} \dot{p} = \left(M - \frac{4}{3} G_u \right) \dot{\epsilon}_z \\ (\dot{\sigma}_z - \dot{\sigma}_r) = \left(\frac{2G_u}{M - \frac{4}{3} G_u} \right) \dot{p} \end{array} \right. \quad (2.9b)$$

$$\text{Unloading and reloading} \quad \left\{ \begin{array}{l} \dot{p} = \left(M - \frac{4}{3} G_u \right) \dot{\epsilon}_z \\ (\dot{\sigma}_z - \dot{\sigma}_r) = \left(\frac{2G_u}{M - \frac{4}{3} G_u} \right) \dot{p} \end{array} \right. \quad (2.9c)$$

$$\text{Unloading and reloading} \quad \left\{ \begin{array}{l} \dot{p} = \left(M - \frac{4}{3} G_u \right) \dot{\epsilon}_z \\ (\dot{\sigma}_z - \dot{\sigma}_r) = \left(\frac{2G_u}{M - \frac{4}{3} G_u} \right) \dot{p} \end{array} \right. \quad (2.9d)$$

Equations 2.9a through d are plotted schematically in Figures 2.2c and d. The material is first loaded (in uniaxial strain configuration) to a stress level corresponding to Point 1 and then unloaded to a stress level corresponding to Point 2.

Figure 2.2c demonstrates an important aspect of the constant shear modulus model when there is no hysteresis in the uniaxial strain curve ($M_\ell = M_u$). Since $G_u > G_\ell$, the unloading slope of the pressure-volumetric strain curve is smaller than the loading slope, i.e.

$$\left(M - \frac{4}{3} G_u \right) < \left(M - \frac{4}{3} G_\ell \right) \quad (2.10)$$

which results in an energy-generating loop in the pressure-volumetric strain curve. This is in direct opposition to the available experimental evidence, which indicates that a true hydrostat would not show an energy-generating loop and the model should not produce one in the constructed pressure-volumetric strain curve.

It should be pointed out that the values of G_ℓ and G_u are not arbitrary. In uniaxial strain tests, it has generally been observed that incremental increases in σ_z are accompanied by increases in σ_r and ϵ_z , that incremental decreases in σ_z result in decreases in σ_r and ϵ_z , and that neither σ_r nor ϵ_z exhibits tensile values while subjected to compressive values of σ_z . Thus, M and K remain positive at all times. This condition restricts both G_ℓ and G_u by requiring that

$$\frac{4}{3} G_\ell < M \quad (2.11a)$$

$$\frac{4}{3} G_u < M \quad (2.11b)$$

Equations 2.11a and b, however, must be replaced by

$$2G_\ell < M \quad (2.11c)$$

$$2G_u < M \quad (2.11d)$$

in order to exclude negative values of Poisson's ratio (Equations 2.7 and 2.8). Therefore, the maximum values of G_ℓ and G_u are fixed by the value of constrained modulus M according to Equations 2.11c and d.

2.3 LINEAR ELASTIC G MODEL FOR MATERIALS WITH A LINEAR HYSTERETIC M

Figures 2.3a and b depict the vertical stress-strain and the principal stress difference-strain difference relations, respectively, for this model under uniaxial strain conditions. Since the shear modulus is linear elastic ($G_\ell = G_u = G$) and the constrained modulus is linear hysteretic ($M_u > M_\ell$), the pressure-volumetric strain and the principal stress

difference-pressure relations for the model are

$$\text{Virgin loading} \quad \left\{ \begin{array}{l} \dot{p} = \left(M_L - \frac{4}{3} G \right) \dot{\epsilon}_z \\ (\dot{\sigma}_z - \dot{\sigma}_r) = \left(\frac{2G}{M_L - \frac{4}{3} G} \right) \dot{p} \end{array} \right. \quad (2.12a)$$

$$\text{Unloading and reloading} \quad \left\{ \begin{array}{l} \dot{p} = \left(M_u - \frac{4}{3} G \right) \dot{\epsilon}_z \\ (\dot{\sigma}_z - \dot{\sigma}_r) = \left(\frac{2G}{M_u - \frac{4}{3} G} \right) \dot{p} \end{array} \right. \quad (2.12c)$$

$$(2.12d)$$

Equations 2.12a through d are plotted schematically in Figures 2.3c and d.

Unlike the previous model, there is no energy-generating loop in the pressure-volumetric strain curve associated with this model (Figure 2.3c). This is due to the fact that $M_u > M_L$, which results in an unloading slope for the pressure-volumetric strain curve that is larger than the loading slope, i.e.

$$\left(M_u - \frac{4}{3} G \right) > \left(M_L - \frac{4}{3} G \right) \quad (2.13)$$

Thus, utilizing a hysteretic constrained modulus in a constant G constitutive model results in a pressure-volumetric strain curve that is qualitatively in agreement with observed behavior. However, the constructed stress path (Figure 2.3d) is contrary to most of the existing experimental data, which generally indicate that the unloading stress path should fall below the loading path. In view of Equations 2.12b, 2.12d, and 2.13, it is clear that unloading stress paths constructed with this type model will always fall above the loading paths.

As discussed for the previous model, the value of G for this model is also restricted by the inequality

$$2G < M_L \quad (2.14)$$

2.4 LINEAR HYSTERETIC G MODEL FOR MATERIALS WITH A LINEAR HYSTERETIC M

Figures 2.4a and b depict the vertical stress-strain and the principal stress difference-strain difference relations, respectively, for this model under uniaxial strain conditions. Both the constrained and shear moduli are linear hysteretic, i.e. $M_u > M_\ell$ and $G_u > G_\ell$. The pressure-volumetric strain relation and the principal stress difference-pressure relation for the model are shown schematically in Figures 2.4c and d. The material is first loaded to a stress level corresponding to Point 1 and then unloaded to a stress level corresponding to Point 2 (Figures 2.4a and b). The constructed pressure-volumetric strain (Figure 2.4c) and principal stress difference-pressure relations (Figure 2.4d), however, may follow Paths 1-A or 1-B upon unloading depending on the relative values of M_ℓ , M_u , G_ℓ , and G_u . If $(M_u - \frac{4}{3}G_u) < (M_\ell - \frac{4}{3}G_\ell)$, the pressure-volumetric strain curve will unload along the Path 1-A resulting in an energy-generating loop, which is contrary to existing experimental data, as was pointed out in Section 2.2. If, on the other hand, $(M_u - \frac{4}{3}G_u) > (M_\ell - \frac{4}{3}G_\ell)$, the pressure-volumetric strain curve will unload along the Path 1-B, which is in general agreement with the available experimental data. The stress difference-pressure relation will unload along Path 1-A, which is contrary to most of the experimental data, if $G_u/(M_u - \frac{4}{3}G_u) < G_\ell/(M_\ell - \frac{4}{3}G_\ell)$ and will unload along Path 1-B if $G_u/(M_u - \frac{4}{3}G_u) > G_\ell/(M_\ell - \frac{4}{3}G_\ell)$. Thus, in order for both the pressure-volumetric strain relation and the principal stress difference-pressure relation to unload along Path 1-B, the following inequalities must be satisfied for the model

$$(M_u - M_\ell) > \frac{4}{3} (G_u - G_\ell) \quad (2.15a)$$

$$\frac{G_u}{G_\ell} > \frac{M_u}{M_\ell} \quad (2.15b)$$

The values of G_ℓ and G_u for this model are also restricted as previously noted by the inequalities

$$2G_l < M_l \quad (2.16a)$$

$$2G_u < M_u \quad (2.16b)$$

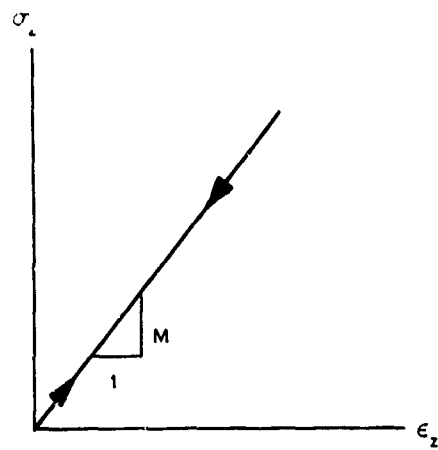
2.5 LINEAR ELASTIC G MODEL FOR MATERIALS WITH A NONLINEAR HYSTERETIC M

Figures 2.5a and b depict the vertical stress-strain and the principal stress difference-strain difference relations, respectively, for this model under uniaxial strain conditions. The pressure-volumetric strain and the principal stress difference-pressure relations for the model are plotted schematically in Figures 2.5c and d. This model is the nonlinear version of the model presented in Section 2.3 and Figure 2.3. Although the principal features of the models are the same, there is an additional feature associated with the nonlinear model that is not evident in a linear model. Since the slope of the stress path varies inversely with the constrained modulus, it follows that the stress path has a curvature that is opposite to that in the corresponding portion of the uniaxial strain curve. This behavior is illustrated in Figure 2.5 by the dashed line A-B. The experimental data obtained to date, however, indicate that the stress path is generally continuously concave to the pressure axis throughout the loading cycle (such as Path A-1 in Figure 2.5d) regardless of the shape of the vertical stress-strain curve.

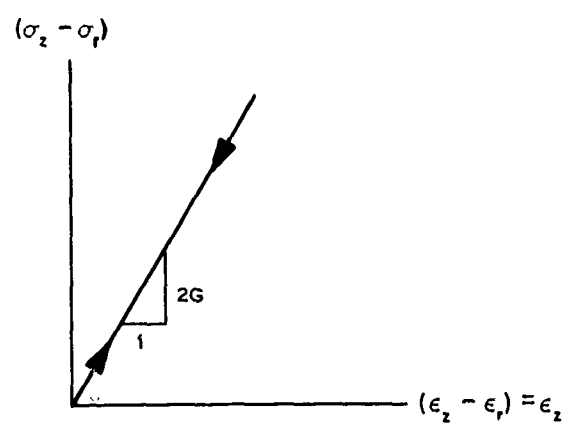
2.6 LINEAR HYSTERETIC G MODEL FOR MATERIALS WITH A NONLINEAR HYSTERETIC M

Figures 2.6a and b depict the vertical stress-strain and the principal stress difference-strain difference relations, respectively. This model is the nonlinear version of the model presented in Section 2.4 and Figure 2.4. The constructed pressure-volumetric strain and the principal stress difference-pressure relations for the model are plotted schematically in Figures 2.6c and d. As discussed in Section 2.4, the constructed pressure-volumetric strain relation (Figure 2.6c) and the principal stress difference-pressure relation (Figure 2.6d) may follow either Path 1-A or Path 1-B upon unloading, depending on the relative values of M_l , M_u , G_l , and G_u .

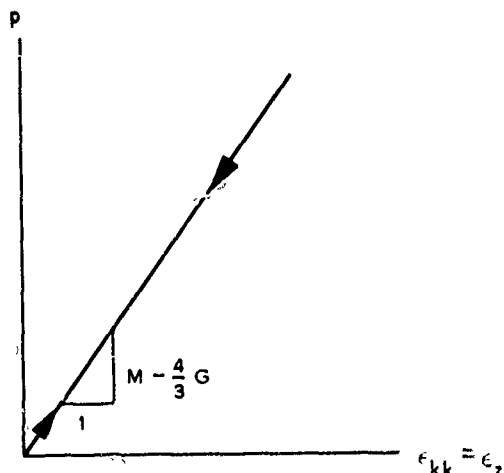
In order for both the pressure-volumetric strain relation and the principal stress difference-pressure relation to unload along Path 1-B, the inequalities given by Equation 2.15 must be satisfied for this model at any stress level. To prevent the occurrence of negative ν values, the values of G_l and G_u must also be restricted by the inequalities given by Equation 2.16 for any stress level.



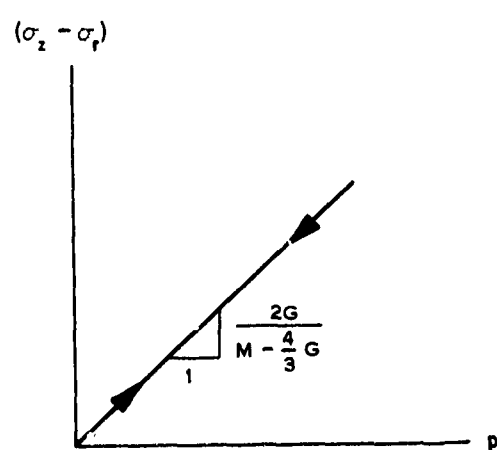
a. VERTICAL STRESS-STRAIN RELATION



b. PRINCIPAL STRESS DIFFERENCE-STRAIN DIFFERENCE RELATION

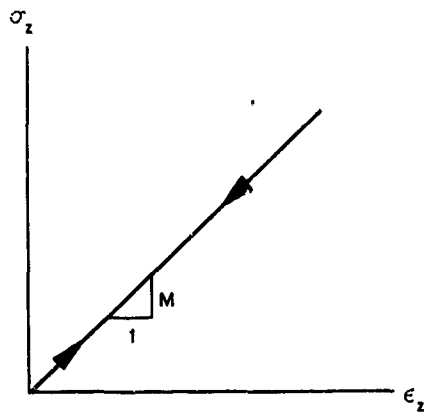


c. PRESSURE-VOLUMETRIC STRAIN RELATION

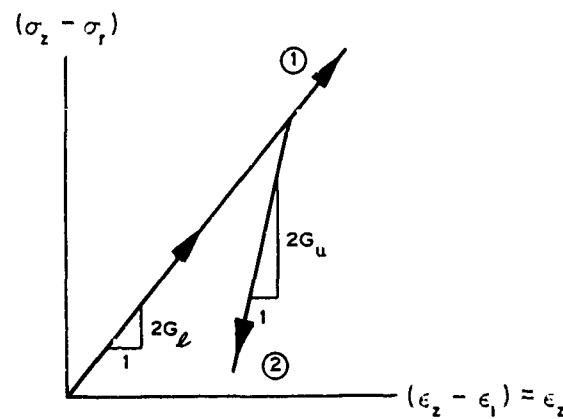


d. PRINCIPAL STRESS DIFFERENCE-PRESSURE RELATION (STRESS PATH)

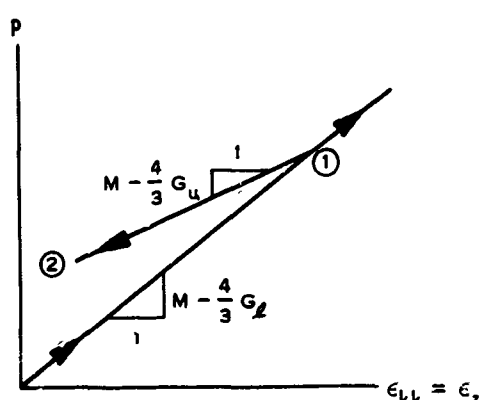
Figure 2.1 Behavior of linear elastic material under conditions of uniaxial strain.



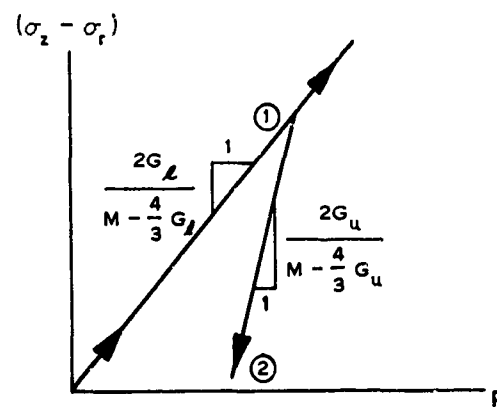
a. VERTICAL STRESS-STRAIN
RELATION



b. PRINCIPAL STRESS DIFFERENCE-
STRAIN DIFFERENCE RELATION

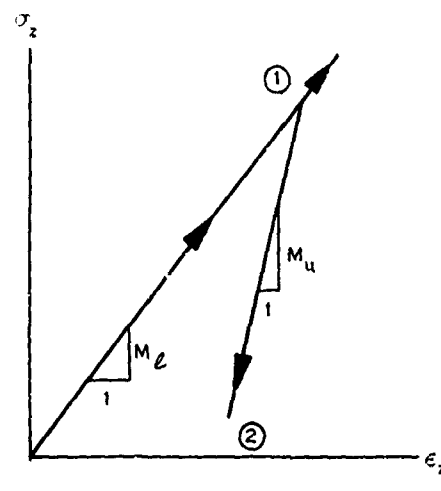


c. PRESSURE-VOLUMETRIC
STRAIN RELATION

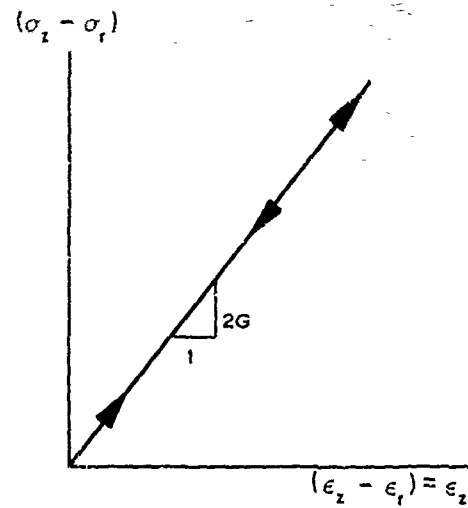


d. PRINCIPAL STRESS DIFFERENCE-
PRESSURE RELATION (STRESS
PATH)

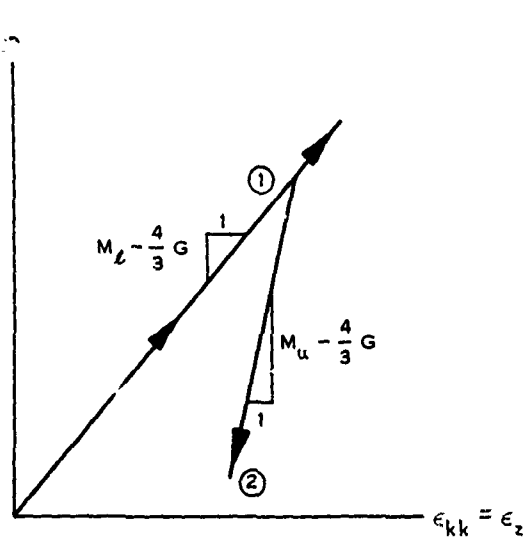
Figure 2.2 Behavior of linear hysteretic shear modulus model for materials with a linear elastic constrained modulus under conditions of uniaxial strain.



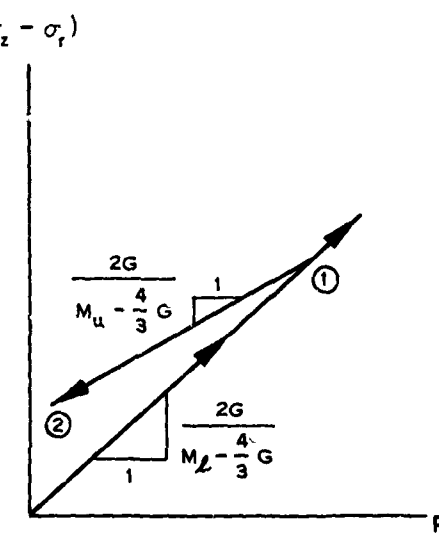
a. VERTICAL STRESS-STRAIN RELATION



b. PRINCIPAL STRESS DIFFERENCE-STRAIN DIFFERENCE RELATION

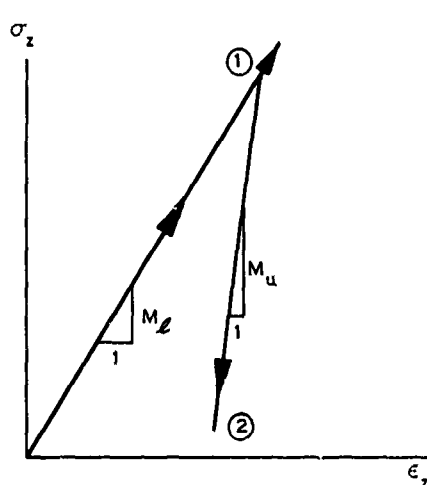


c. PRESSURE-VOLUMETRIC STRAIN RELATION

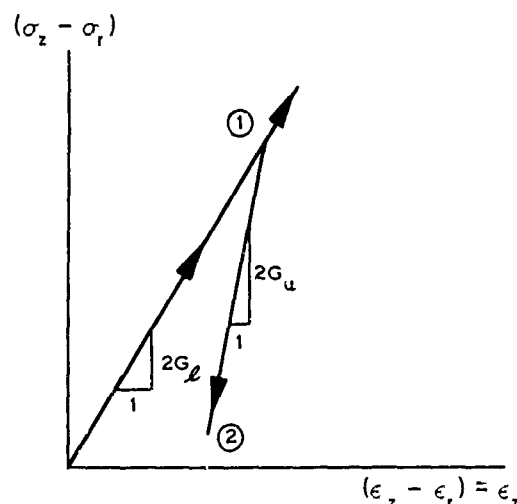


d. PRINCIPAL STRESS DIFFERENCE-PRESSURE RELATION (STRESS PATH)

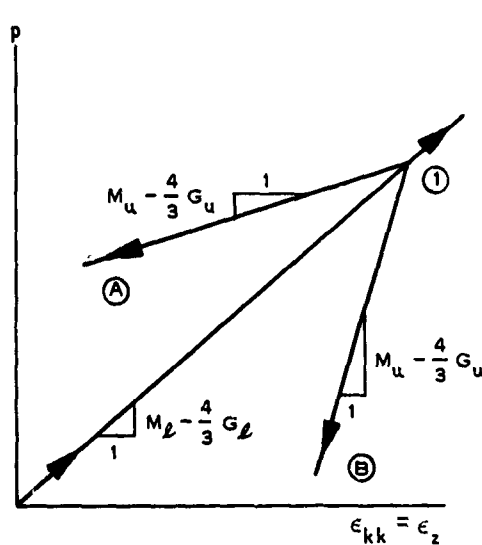
Figure 2.3 Behavior of linear elastic shear modulus model for materials with a linear hysteretic constrained modulus under conditions of uniaxial strain.



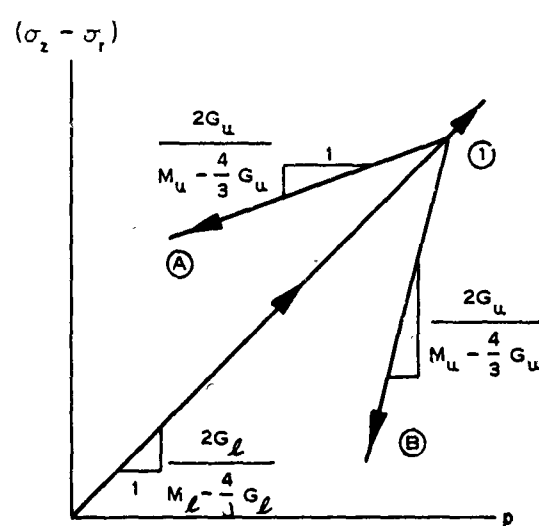
a. VERTICAL STRESS-STRAIN
RELATION



b. PRINCIPAL STRESS DIFFERENCE-
STRAIN DIFFERENCE RELATION

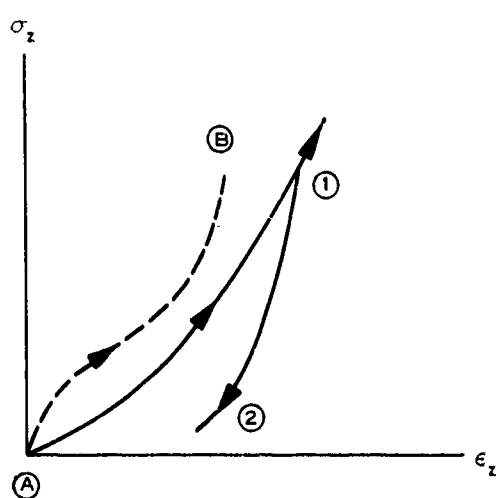


c. PRESSURE-VOLUMETRIC
STRAIN RELATION

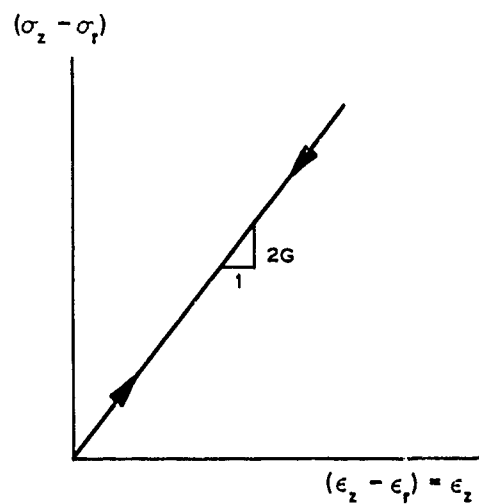


d. PRINCIPAL STRESS DIFFERENCE-
PRESSURE RELATION (STRESS
PATH)

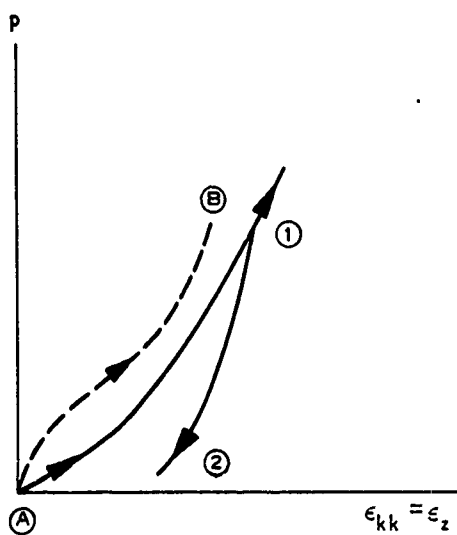
Figure 2.4 Behavior of linear hysteretic shear modulus model for materials with a linear hysteretic constrained modulus under conditions of uniaxial strain.



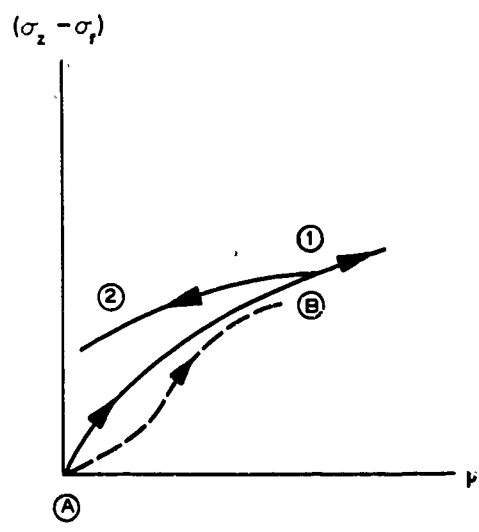
a. VERTICAL STRESS-STRAIN
RELATION



b. PRINCIPAL STRESS DIFFERENCE-
STRAIN DIFFERENCE RELATION

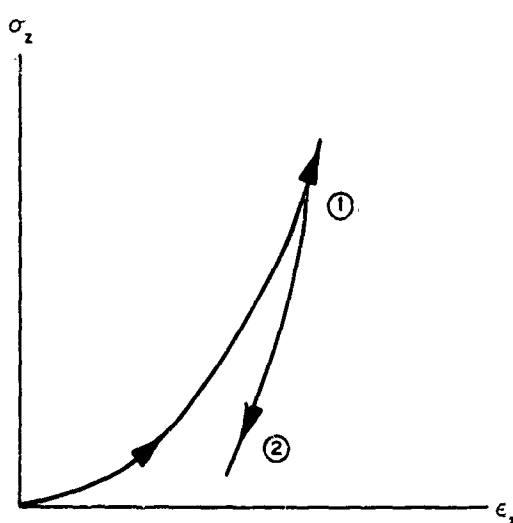


c. PRESSURE-VOLUMETRIC
STRAIN RELATION

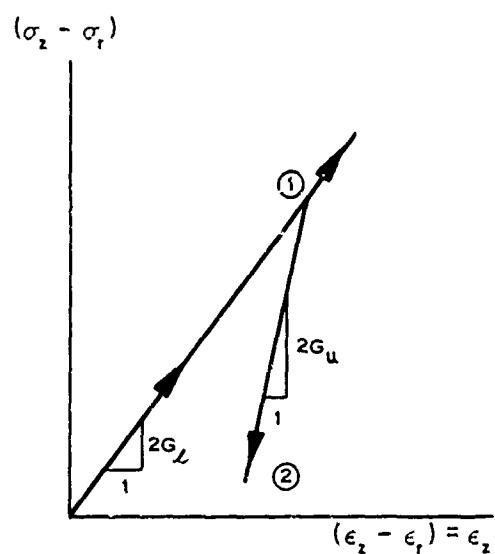


d. PRINCIPAL STRESS DIFFERENCE-
PRESSURE RELATION (STRESS
PATH)

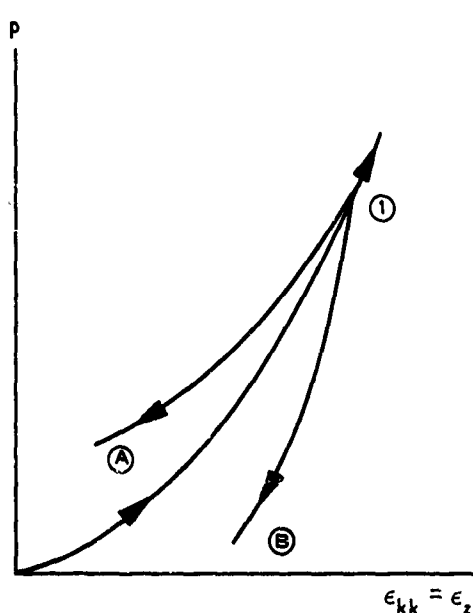
Figure 2.5 Behavior of linear elastic shear modulus model for materials with a nonlinear hysteretic constrained modulus under conditions of uniaxial strain.



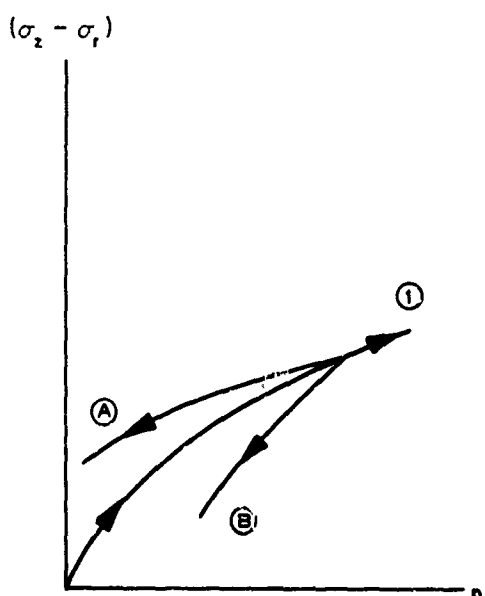
a. VERTICAL STRESS-STRAIN RELATION



b. PRINCIPAL STRESS DIFFERENCE-
STRAIN DIFFERENCE RELATION



c. PRESSURE-VOLUMETRIC
STRAIN RELATION



d. PRINCIPAL STRESS DIFFERENCE-
PRESSURE RELATION (STRESS
PATH)

Figure 2.6 Behavior of linear hysteretic shear modulus model for materials with a nonlinear hysteretic constrained modulus under conditions of uniaxial strain.

CHAPTER 3
CONSTANT SHEAR MODULUS CONSTITUTIVE MODELS FOR
STRESS STATES REACHING YIELD

The procedure used to construct the various constant G models discussed in this chapter is basically the same as that described in Chapter 2. The distinction between the two procedures becomes apparent only when a stress state satisfying the von Mises yield condition ($\sqrt{J_2} = k$) is obtained. When such a stress state is reached, the value of shear modulus becomes effectively equal to zero and the constrained and bulk moduli become equal. Two different models are considered in this chapter as outlined in Section 1.2.

3.1 LINEAR ELASTIC G MODEL FOR MATERIALS WITH A BILINEAR HYSTERETIC M

Figure 3.1a depicts the vertical stress-strain relation for this model under uniaxial strain conditions. The loading portion of the stress-strain curve is approximated with two straight lines having slopes M_l^1 and M_l^2 where $M_l^2 > M_l^1$. The unloading part of the curve is also represented by two straight lines with slopes M_u^1 and M_u^2 where $M_u^1 > M_u^2$. The principal stress difference-strain difference relation for the model is shown in Figure 3.1b. The material first behaves as a linear elastic G model with a linear hysteretic constrained modulus (Section 2.3) until a stress state corresponding to the von Mises yield limit k is reached. This corresponds to Point 1 in Figure 3.1. Physically, Point 1 is often associated with the forcing of entrapped air into solution and the subsequent saturation of the soil specimen, which results in a stiffer behavior in uniaxial strain or hydrostatic compression and a weaker behavior in shear.

Upon yielding, the material behaves as though it were a constrained fluid exhibiting no shear resistance. The slope of the vertical stress-strain curve breaks at Point 1 and becomes equal to M_l^2 . The slope of the principal stress difference-strain difference curve also breaks at Point 1 and becomes equal to zero. The stress difference and vertical stress magnitudes at Point 1 are, respectively, $\sqrt{3} k$ and $\sqrt{3} k M_l^1 / 2G$.

During unloading from a stress state corresponding to Point 2 (Figures 3.a and b), the material behaves as a linear elastic solid in shear ($G_\ell = G_u = G$), but since $M_u^1 > M_\ell^2$, it exhibits hysteretic effects in the hydrostatic part of its deformation unless $M_u^1 - \frac{4}{3}G = M_\ell^2$. When the lower yield surface corresponding to Point 3 is reached, the material again flows plastically. The slope of the vertical stress-strain curve breaks at Point 3 and becomes equal to M_u^2 and the slope of the principal stress difference-strain difference curve becomes equal to zero. Since $M_u^2 > M_\ell^1$, hysteretic volume change continues to increase with subsequent further unloading.

Equation 2.1 can now be utilized to calculate the pressure-volumetric strain and the stress difference-pressure relations associated with a state of uniaxial strain. During loading from Point 0 to Point 1 (Figure 3.1), the pressure-volumetric strain and the stress difference-pressure relations become

$$\dot{p} = \left(M_\ell^1 - \frac{4}{3}G \right) \dot{\epsilon}_z \quad (3.1a)$$

$$(\dot{\sigma}_z - \dot{\sigma}_r) = \left(\frac{2G}{M_\ell^1 - \frac{4}{3}G} \right) \dot{p} \quad (3.1b)$$

Equations 3.1a and b apply only up to Point 1, which corresponds to

$$p = \frac{\sqrt{3}}{2} k \left(M_\ell^1 - \frac{4}{3}G \right) \quad (3.2a)$$

$$(\sigma_z - \sigma_r) = \sqrt{3}k \quad (3.2b)$$

During loading from Point 1 to a stress state corresponding to Point 2, the material flows plastically and the shear modulus becomes effectively equal to zero. Accordingly, the pressure-volumetric strain relation becomes

$$\dot{p} = M_\ell^2 \dot{\epsilon}_z \quad (3.3)$$

During unloading from Point 2 to a stress state corresponding to Point 3, the material behaves elastically in shear resulting in the following stress difference-pressure relation

$$(\dot{\sigma}_z - \dot{\sigma}_r) = \left(\frac{2G}{M_u^1 - \frac{4}{3}G} \right) \dot{p} \quad (3.4)$$

At Point 3, the yield surface is intersected again, this time on its "lower" side so that

$$(\sigma_z - \sigma_r) = -\sqrt{3} k \quad (3.5)$$

The pressure-volumetric strain curve, however, may unload along Paths 2-A or 2-B as shown in Figure 3.1c, depending on the relative values of the constrained and shear moduli used for the model. The mathematical expression describing the pressure-volumetric strain relation for the stress range between Points 2 and 3 is given by

$$\dot{p} = \left(M_u^1 - \frac{4}{3} G \right) \dot{\epsilon}_z \quad (3.6)$$

If $\left(M_u^1 - \frac{4}{3} G \right) < M_\ell^2$, the pressure-volumetric strain curve will unload along Path 2-A, resulting in an energy-generating loop, which contradicts available experimental data. If, on the other hand, $\left(M_u^1 - \frac{4}{3} G \right) > M_\ell^2$, the pressure-volumetric strain curve will unload along Path 2-B, which is in general agreement with current experimental data. If unloading is continued beyond Point 3, the material flows plastically again and the pressure-volumetric strain relation becomes

$$\dot{p} = M_u^2 \dot{\epsilon}_z \quad (3.7)$$

Equations 3.1 through 3.7 completely describe the behavior of the model under conditions of uniaxial strain. In order to avoid an energy-generating loop in the pressure-volumetric strain relation, the constrained and shear moduli must be restricted by the following inequality

$$\left(M_u^1 - M_\ell^2 \right) > \frac{4}{3} G \quad (3.8)$$

To avoid negative values of v , the value of G is further restricted by the inequality

$$2G < M_\ell^1 \quad (3.9)$$

3.2 LINEAR ELASTIC G MODEL FOR MATERIALS WITH A NONLINEAR HYSTERETIC M

This model is the nonlinear version of the bilinear hysteretic model presented in Section 3.1. Figures 3.2a and b show the vertical stress-strain and the principal stress difference-strain difference relations, respectively, for this model under conditions of uniaxial strain. The material first behaves as a linear elastic G model with a nonlinear hysteretic constrained modulus (Section 2.5) until the plastic yield stress is reached. This corresponds to Point 1 in Figure 3.2. Upon yielding, the slope of the principal stress difference-strain difference curve breaks and becomes equal to zero. The slope of the vertical stress-strain curve, however, increases with continued application of vertical stress. The magnitude of the stress difference at Point 1 is $\sqrt{3} k$, where k is the von Mises yield limit. The magnitude of the vertical stress at Point 1 is the value of σ_z corresponding to $\epsilon_z = \frac{\sqrt{3}k}{2G}$. During unloading from a stress state corresponding to Point 2, the material behaves as a linear elastic solid in shear and exhibits nonlinear hysteretic behavior in the hydrostatic part of the deformation, until the lower yield surface corresponding to Point 3 is reached. The slope of the stress difference-strain difference curve breaks again at Point 3 and becomes equal to zero. The slope of the vertical stress-strain curve continuously decreases with further unloading of the vertical stress beyond Point 3.

This description of the vertical stress-strain relation is more realistic than the bilinear representation presented in Section 3.1. Since the constrained modulus in this case depends on the stress level, the construction of the model must be carried out incrementally utilizing Equations 2.3 and 2.4 and imposing the condition that $(\dot{\sigma}_z - \dot{\sigma}_r) = 0$ on the yield surface.

The constructed pressure-volumetric strain and stress difference-pressure relations for the model are plotted schematically in Figures 3.2c and d, respectively. In order for the pressure-volumetric strain curve (Figure 3.2c) to avoid exhibiting an energy-generating loop and to unload along Path 2-B, the following inequality must hold in any stress increment

$$\left(M_u - M_\ell \right) > \frac{4}{3} G \quad (3.10)$$

As was pointed out previously, the above inequality insures that the unloading slope of the pressure-volumetric curve is greater than the corresponding loading slope in any stress increment. The shear modulus is further restricted to positive values of ν by the inequality

$$2G < M_\ell \quad (3.11)$$

in any stress increment. When coupled with Equation 1.4, the above inequality also restricts the slopes along the uniaxial strain-stress paths plotted in principal stress difference versus pressure space to positive values less than 3, i.e.

$$\left(\frac{\dot{\sigma}_z - \dot{\sigma}_r}{\dot{p}} \right)_{\text{uniaxial strain}} < 3 \quad (3.12)$$

The stress path in Figure 3.2d has a curvature in the elastic range (Path 0-1) that is opposite to that in the corresponding portion of the vertical stress-strain curve (Figure 3.2a). Thus, while the vertical stress-strain curve stiffens as pressure increases, the stress path softens until the material yields. The unloading stress path between Points 2 and 3 for this model approaches a straight line at high pressures where the unloading constrained modulus is essentially linear and becomes convex to the pressure axis at low pressure where the hook or tail in the vertical stress-strain curve starts developing. Thus, if the constrained modulus is continuously hardening, the slope of the calculated stress path is continuously reduced; if the constrained modulus softens, the calculated stress path becomes progressively steeper. This latter calculated curvature when unloading reaches low pressure is in direct contrast with available experimental uniaxial strain-stress path data.

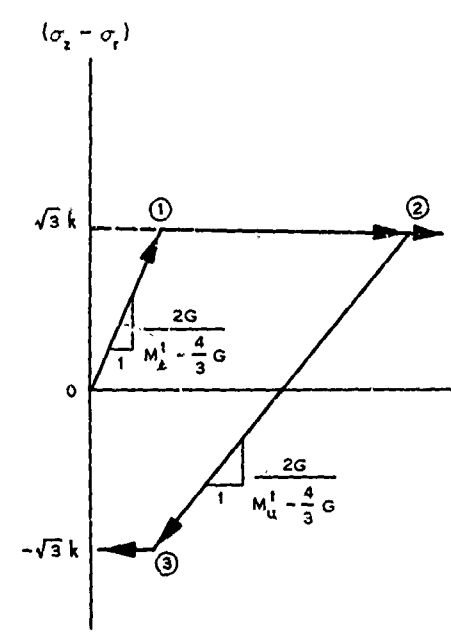
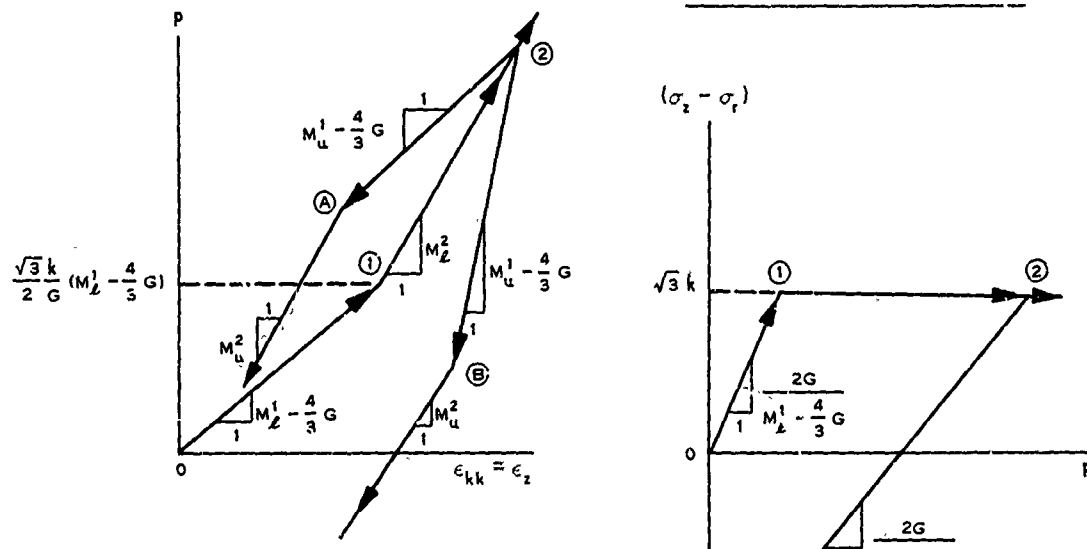
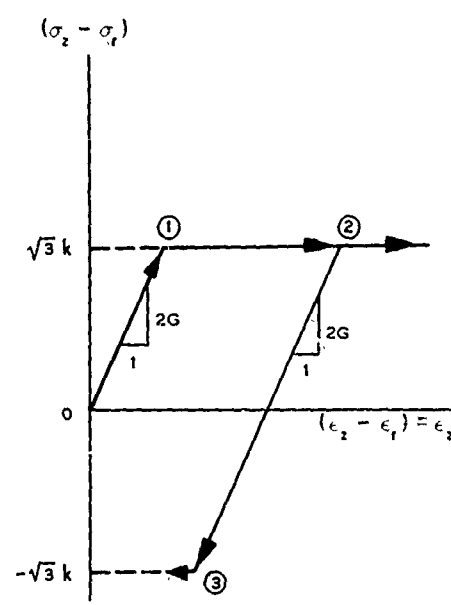
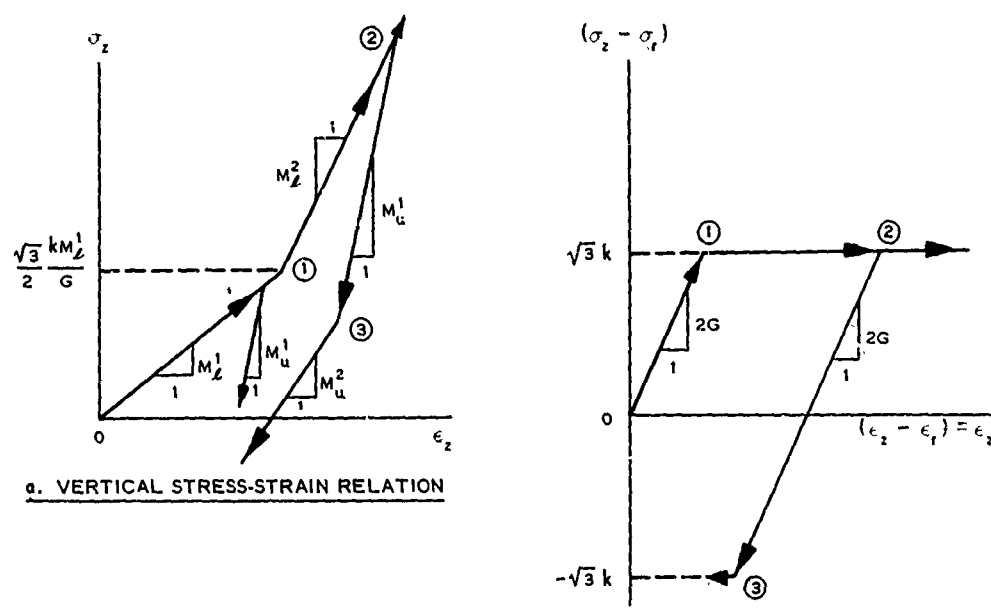
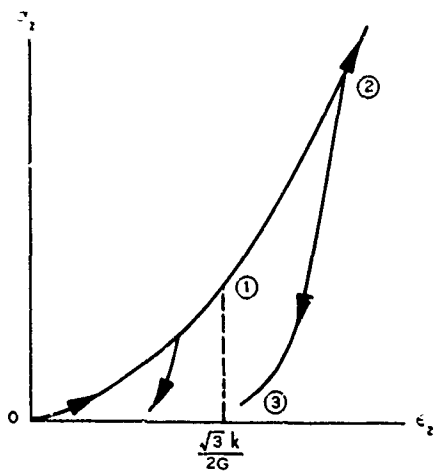
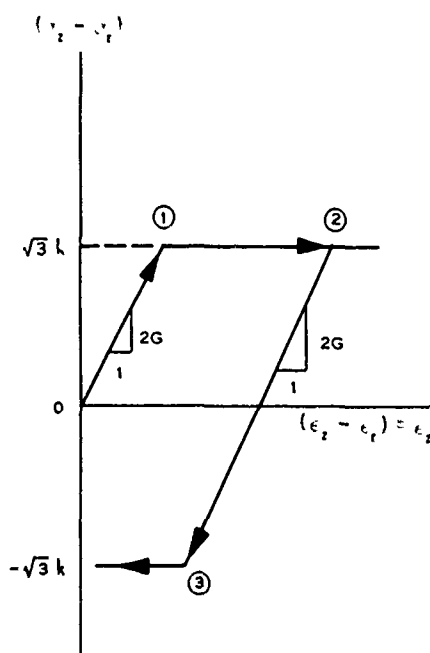


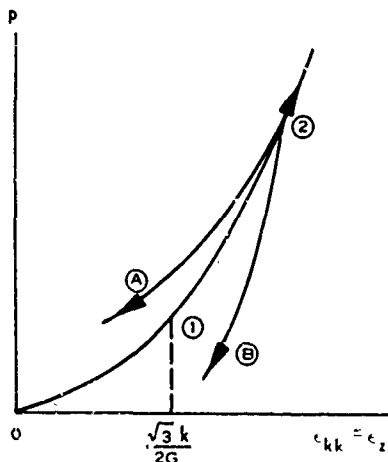
Figure 3.1 Behavior of linear elastic shear modulus model for elastic-plastic materials with a bilinear hysteretic constrained modulus under conditions of uniaxial strain.



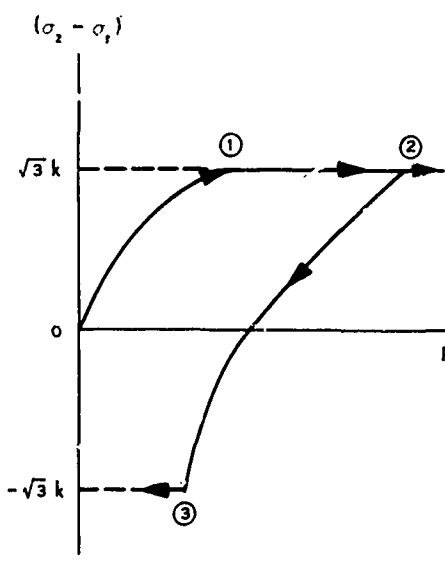
a. VERTICAL STRESS-STRAIN RELATION



b. PRINCIPAL STRESS DIFFERENCE-
STRAIN DIFFERENCE RELATION



c. PRESSURE-VOLUMETRIC
STRAIN RELATION



d. PRINCIPAL STRESS DIFFERENCE-
PRESSURE RELATION (STRESS
PATH)

Figure 3.2 Behavior of linear elastic shear modulus model for elastic-plastic materials with a nonlinear hysteretic constrained modulus under conditions of uniaxial strain.

CHAPTER 4

CONCLUSIONS AND RECOMMENDATIONS

4.1 CONCLUSIONS

The results from this simple examination of several highly idealized material descriptions indicate that many of the behavior characteristics of real earth materials often recorded during laboratory tests can be simulated, at least qualitatively, by elastic-plastic constitutive models of the constant G-type by observing certain restrictions on the material property parameters G and M . Other characteristic phenomena, however, cannot be mirrored with this type model under any circumstances.

For example, even if M_u is always greater than M_ℓ at any stress level, only by utilizing the linear hysteretic G model and observing the following inequalities,

$$(M_u - M_\ell) > \frac{4}{3} (G_u - G_\ell) \quad \text{and} \quad \frac{G_u}{G_\ell} > \frac{M_u}{M_\ell}$$

can one insure that pressure-volumetric strain curves will be constructed that exhibit energy-absorbing hysteretic behavior rather than energy-generating loops when unloaded from any stress level. These same inequalities must also be adhered to if unloading paths of principal stress difference versus pressure for a state of uniaxial strain are to fall below the loading path rather than above it. In order to be consistent with the experimental observation that axial and radial stresses simultaneously increase or decrease during loading or unloading, respectively, and also restrict Poisson's ratio values to be greater than zero at any stress level, it is necessary to observe the inequalities

$$2G_\ell < M_\ell \quad \text{and} \quad 2G_u < M_u$$

The linear hysteretic G model will obviously incorporate the well known ability of soils to dissipate energy in shear, even at subyield stress levels.

Uniaxial strain tests on undisturbed natural soils, however, usually

reveal a reversal of curvature in σ_z versus ϵ_z plots during loading, first softening and then hardening, while the corresponding $(\sigma_z - \sigma_r)$ versus p plots generally indicate monotonically softening behavior. Any constant G model, however, if coupled with a loading constrained modulus that reverses curvature, will of necessity have a curvature reversal during loading in its $(\sigma_z - \sigma_r)$ versus p curve, unless a plastic yield criterion is invoked at a pressure level less than that of the inflection point. On the other hand, reversals of curvature have never been observed in plots of unloading constrained moduli; yet unloading stress paths frequently exhibit directional changes in curvature. Again, if the constrained modulus unloading curvature does not change sign, then the unloading stress path curvature calculated with any constant G model cannot. In fact, when unloading reaches low pressure or approaches the lower-bound or negative plastic yield limit, the constant G calculated stress path curvature is always in direct contrast with available experimental uniaxial strain test data.

While it is obvious that elastic-plastic constitutive models formulated with constant values of G can match some of the dominant features exhibited by soils and weak rocks during uniaxial strain tests, it is equally obvious that some features can only be mirrored in a limited fashion and others not at all. It is also quite obvious that any model that is linear in G cannot possibly exhibit the nonlinear stress-strain behavior usually observed during triaxial compression tests.

4.2 RECOMMENDATIONS

Thus, it is recommended that research efforts to develop realistic mathematical constitutive models of earth media for use in free-field ground shock calculation codes continue. In the authors' opinion, such efforts should be governed by the following criteria:

1. The models should be capable of qualitatively and quantitatively matching the salient nonlinear and hysteretic response characteristics of earth media, not only as determined from the uniaxial strain test, but also as determined from a variety of other laboratory test boundary conditions. If confidence is to be placed in a ground shock code which must calculate earth material response to an unknown number of varying states of stress,

transient boundary loadings, and erratic site geometries, the material model used should at least have the capability to reasonably duplicate the response of relatively homogeneous specimens of simplified geometries loaded in the laboratory along known stress paths under carefully controlled conditions.

2. The numerical values of the coefficients defining the models should be readily derivable from laboratory test data. It is most important that the coefficient values not be merely a set of numbers generated through a trial and error "black box" routine to fit a given set of data, but that they have physical significance in terms of compressibility, shear strength, etc., so that when extrapolating to different materials, rational engineering judgments can be made as to their relative magnitudes based on geologic descriptions, mechanical properties, and other conventional indexes.

3. Theoretical restrictions, such as those imposed by uniqueness and continuity considerations, should be satisfied to the maximum practicable extent. It should be kept in mind, however, that earth materials are almost invariably nonhomogeneous, anisotropic, stress-history dependent, chemically entangled mixtures of gases, liquids, and solid particles. Therefore, it seems unreasonable to expect that constitutive models for these materials can be developed which satisfy all the mathematical restrictions imposed through assumption of formal continuous media theories while accurately mirroring all of the details observed during various laboratory tests. Obviously, some compromises will inevitably have to be made; parametric studies to evaluate the relative importance of ignoring certain features of either data or theory are needed.

4. Any ground shock prediction technique or code should be thoroughly checked against the available analytical solutions and a variety of actual field experiments. Efforts to incorporate new constitutive models into generalized codes for calculating transient ground shock effects from explosive events should also include attempts to obtain analytical or closed-form solutions to special problems of wave propagation through materials containing the principal features of the new models. Presumably, improved models should provide improved correlations with existing field data.

The above criteria are admittedly more pragmatic than theoretical. However, the authors strongly believe that any critical analysis of material models should include examination in the light of all these criteria in order to maintain a balance in perspective.

APPENDIX A

CONSTITUTIVE EQUATIONS AND UNIAXIAL STRAIN BEHAVIOR FOR A PRANDTL-REUSS MATERIAL

A.1 PURPOSE

When constructing constitutive models to represent the rather complicated nonlinear hysteretic behavior of real earth materials using incremental stress-strain relations based on classical elastic-plastic theory, it is helpful to review the equations governing the behavior of an ideal elastic-plastic material and examine its response under typical test boundary conditions.

The purpose of this appendix is to perform such a function for perhaps the most widely known ideal elastic-plastic material, i.e. the Prandtl-Reuss material, and the most useful test conditions for blast-oriented problems, i.e. loading and unloading states of uniaxial strain.

A.2 CONSTITUTIVE EQUATIONS

A.2.1 Yield Criterion. The yield criterion associated with the Prandtl-Reuss material is the well-known von Mises criterion given by

$$\sqrt{J_2} = k \quad (\text{A.1})$$

where k is a material constant related to the cohesive strength of the material. Equation A.1 describes a right-circular cylinder in the principal stress space with its central axis the line of hydrostatic stress as shown in Figure A.1.

According to the basic postulate of the plasticity theory, the material would flow plastically, undergoing plastic as well as elastic strains when Equation A.1 is satisfied. The total strain is then the sum of the elastic (recoverable) strain and plastic or permanent strain. When the stresses are less than those satisfying Equation A.1, the material will undergo elastic strains only; i.e., the material behaves as a linear elastic solid. In incremental notation, these conditions can be written as

$$\left. \begin{array}{l} \dot{\epsilon}_{ij}^e = \dot{\epsilon}_{ij}^e \quad \text{when } \sqrt{J_2^t} < k \\ \dot{\epsilon}_{ij}^p = \dot{\epsilon}_{ij}^e + \dot{\epsilon}_{ij}^p \quad \text{when } \sqrt{J_2^t} = k \end{array} \right\} \quad (\text{A.2})$$

where $\dot{\epsilon}_{ij}^e$ = components of elastic strain increment tensor

$\dot{\epsilon}_{ij}^p$ = components of plastic strain increment tensor

According to Hooke's law, the elastic strain increment tensor is given by

$$\dot{\epsilon}_{ij}^e = \frac{1+\nu}{E} \dot{\sigma}_{ij} - \frac{\nu}{E} \dot{\sigma}_{kk} \delta_{ij} \quad (\text{A.3})$$

where E = Young's modulus of elasticity.

The plastic strain increment tensor can be derived from the yield criterion (Equation A.1) by utilizing the theory of plastic potential:

$$\dot{\epsilon}_{ij}^p = \lambda \frac{\partial f}{\partial \sigma_{ij}} \quad (\text{A.4})$$

where λ = a positive scalar factor of proportionality

$$f = J_2^t - k^2$$

A.2.2 Stress-Strain Relationship. In view of Equation A.4 and the function f , the plastic strain increment tensor becomes

$$\dot{\epsilon}_{ij}^p = \lambda \frac{\partial (J_2^t - k^2)}{\partial \sigma_{ij}} = \lambda s_{ij} \quad (\text{A.5})$$

Since $s_{kk} = 0$, it follows from Equation A.5 that

$$\dot{\epsilon}_{kk}^p = 0 \quad (\text{A.6})$$

indicating that no plastic volume change can occur in the plastic range for Prandtl-Reuss material. Hence, all volume change is elastic, i.e.

$$\dot{\epsilon}_{kk} = \dot{\epsilon}_{kk}^e \quad (\text{A.7})$$

and

$$\dot{\epsilon}_p = K \dot{\epsilon}_{kk}^e \quad (A.8)$$

Accordingly, the plastic deviator strain increment tensor $\dot{\epsilon}_{ij}^p$ is the same as the plastic strain increment tensor $\dot{\epsilon}_{ij}^p$. The total deviator strain increment tensor $\dot{\epsilon}_{ij}$ then becomes

$$\dot{\epsilon}_{ij} = \dot{\epsilon}_{ij}^e + \dot{\epsilon}_{ij}^p \quad (A.9)$$

where $\dot{\epsilon}_{ij}^e = \dot{s}_{ij}/2G$ = components of elastic deviator strain increment tensor. Employing Equation A.5 in Equation A.9 results in the following relation for the total deviator strain increment tensor

$$\dot{\epsilon}_{ij} = \frac{\dot{s}_{ij}}{2G} + \lambda s_{ij} \quad (A.10)$$

Multiplying both sides of Equation A.10 by $2Gs_{ij}$ yields

$$2Gs_{ij} \dot{\epsilon}_{ij} = \dot{s}_{ij} s_{ij} + \lambda 2Gs_{ij} s_{ij} \quad (A.11)$$

or

$$2G\dot{W} = \dot{J}_2' + 4G\lambda J_2' \quad (A.12)$$

where $\dot{W} = s_{ij} \dot{\epsilon}_{ij}$ = the rate of work or increment of internal energy due to distortion and $J_2' = s_{ij} \dot{s}_{ij}$. Since $J_2' = k^2$ = constant during yielding, $\dot{J}_2' = 0$ and Equation A.12 yields the following relation for the proportionality factor λ

$$\lambda = \frac{\dot{W}}{2k} \quad (A.13)$$

It is to be noted that \dot{W} is only due to plastic deformation. In view of Equation A.13, the total deviator strain increment tensor (Equation A.10) takes the following form

$$\dot{e}_{ij} = \frac{1}{2G} \left(\dot{s}_{ij} + \frac{GW}{k^2} s_{ij} \right) \quad (A.14)$$

Equation A.14 can be inverted to solve for the deviator stress increment tensor \dot{s}_{ij} , i.e.

$$\dot{s}_{ij} = 2G \left(\dot{e}_{ij} - \frac{\dot{W}}{2k^2} s_{ij} \right) \quad (A.15)$$

Equation A.15 (or Equation A.14) is the Prandtl-Reuss stress-strain relation; it applies in the plastic range when $J_2' = k^2$ and $\dot{W} > 0$. If $\dot{W} < 0$, unloading is taking place, i.e. the behavior is only elastic and Equation A.3 applies. If $\dot{W} = 0$ the loading is said to be neutral.

The above results can be summarized in the following form

$$\left\{ \begin{array}{l} \dot{e}_{ij} = \frac{\dot{s}_{ij}}{2G} \quad \text{when} \quad \sqrt{J_2'} < k \quad (\text{elastic loading}) \\ \dot{e}_{ij} = \frac{1}{2G} \left(\dot{s}_{ij} + \frac{GW}{k^2} s_{ij} \right) \quad \text{when} \quad \sqrt{J_2'} = k, \dot{W} > 0 \end{array} \right. \quad (A.16a)$$

$$\left\{ \begin{array}{l} \dot{e}_{ij} = \frac{\dot{s}_{ij}}{2G} \quad \text{when} \quad \dot{W} < 0 \quad (\text{elastic unloading}) \end{array} \right. \quad (A.16b)$$

$$\left\{ \begin{array}{l} \dot{e}_{ij} = \frac{\dot{s}_{ij}}{2G} \quad \text{when} \quad \dot{W} < 0 \quad (\text{elastic unloading}) \end{array} \right. \quad (A.16c)$$

In order to obtain the components of the stress increment tensor $\dot{\sigma}_{ij}$, Equation A.16 must be combined with Equation A.8.

A.3 BEHAVIOR UNDER CONDITIONS OF UNIAXIAL STRAIN

For uniaxial strain conditions in a cylindrical coordinate system r, θ, z , the following boundary conditions prevail (Figure A.2)

$$\left. \begin{array}{l} \epsilon_r = \epsilon_\theta = 0 \\ \epsilon_r = \epsilon_\theta = -\frac{1}{3}\epsilon_z \\ \epsilon_z = \frac{2}{3}\epsilon_z \end{array} \right\} \quad (A.17)$$

In the elastic range, the behavior of the material is governed by Equation A.3, which can also be written in the following form

$$\dot{\epsilon}_{ij} = \frac{s_{ij}}{2G} + \frac{p}{3K} \delta_{ij} \quad (A.18)$$

Since $\dot{\epsilon}_r = \dot{\epsilon}_\theta = 0$, Equation A.18 yields the following relations between components of deviator stress increment and \dot{p}

$$\dot{s}_r = \dot{s}_\theta = - \frac{2G}{3K} \dot{p} \quad (A.19)$$

In view of the fact that $s_{kk} = 0$, Equation A.19 gives

$$\dot{s}_z = -2\dot{s}_r = \frac{4G}{3K} \dot{p} \quad (A.20)$$

Utilizing the relation $\dot{s}_z = \dot{\sigma}_z - \dot{p}$ in Equation A.20 results in the following relation for the vertical stress increment $\dot{\sigma}_z$

$$\dot{\sigma}_z = \left(\frac{3K + 4G}{3K} \right) \dot{p} \quad (A.21)$$

Since for uniaxial strain conditions $\dot{\epsilon}_{kk} = \dot{\epsilon}_z$, and in view of Equations A.7 and A.8, the vertical stress-strain increment relation in the elastic range becomes

$$\dot{\sigma}_z = \left(K + \frac{4}{3} G \right) \dot{\epsilon}_z = M \dot{\epsilon}_z \quad (A.22)$$

From Equation A.19, the principal stress difference, in incremental form, is

$$(\dot{\sigma}_z - \dot{\sigma}_r) = \frac{2G}{K} \dot{p} \quad (A.23a)$$

indicating that the slope of the uniaxial strain-stress path in the elastic range is equal to $2G/K$. From the relations between constants in elastic theory, it can readily be shown that

$$\frac{2G}{K} = \frac{3(1 - 2\nu)}{(1 + \nu)} \quad (A.23b)$$

which, when coupled with Equation A.23a, gives the following relation for the condition of uniaxial strain

$$\dot{\sigma}_r = \frac{v}{1-v} \dot{\sigma}_z \quad (A.24)$$

In view of Equations A.8, A.17, and A.23, the principal stress difference-strain difference relation for uniaxial strain becomes

$$(\dot{\sigma}_z - \dot{\sigma}_r) = 2G(\dot{\epsilon}_z - \dot{\epsilon}_r) = 2G\dot{\epsilon}_z \quad (A.25)$$

For virgin loading in the elastic range, Equations A.17 through A.25 can be used without the dot notation.

In the uniaxial strain test

$$\sqrt{J_2^t} = \frac{1}{\sqrt{3}} (\sigma_z - \sigma_r) \quad (A.26)$$

Thus the material will yield when

$$\frac{1}{\sqrt{3}} (\sigma_z - \sigma_r) = k \quad (A.27)$$

In view of Equations 2.8, A.24, and A.27, the value of vertical stress σ_z at yield becomes

$$\sigma_z = \frac{\sqrt{3}M}{2G} k \quad (A.28)$$

Thus, when σ_z reaches the value given by Equation A.28, the material yields and the continued application of vertical stress causes the material to move along the yield surface undergoing plastic as well as elastic strains. In the plastic range Equations A.18 through A.25 no longer apply and recourse to Equations A.8 and A.15 is necessary.

According to Equation A.15, the deviator stress increment \dot{s}_z in the plastic range is given by

$$\dot{s}_z = 2G\dot{\epsilon}_z - \frac{Gw}{k^2} s_z \quad (A.29)$$

The rate of work \dot{W} for conditions of uniaxial strain reduces to

$$\dot{W} = s_z \dot{\epsilon}_z + 2s_r \dot{\epsilon}_r \quad (A.30)$$

or, utilizing the fact that $s_{kk} = c_{kk} = 0$,

$$\dot{W} = \frac{3}{2} s_z \dot{\epsilon}_z \quad (A.31)$$

Substituting Equation A.31 into Equation A.29 and utilizing the relation $\dot{\epsilon}_z = \frac{2}{3} \dot{\epsilon}_z$ results in the following expression for \dot{s}_z

$$\dot{s}_z = \frac{4G}{3} \dot{\epsilon}_z - \frac{G}{k^2} s_z^2 \dot{\epsilon}_z \quad (A.32)$$

In the plastic range

$$k^2 = J_2^1 = \frac{1}{3} (\sigma_z - \sigma_r)^2 = \frac{3}{4} s_z^2 \quad (A.33)$$

and Equation A.32 reduces to

$$\dot{s}_z = \frac{4}{3} G \dot{\epsilon}_z - \frac{4}{3} G \dot{\epsilon}_z = 0 \quad (A.34)$$

Since $\dot{s}_z = 0$, $\dot{s}_r = 0$ also, and

$$\dot{\sigma}_z = \dot{s}_z + \dot{p} = \dot{p} \quad (A.35a)$$

$$\dot{\sigma}_r = \dot{\sigma}_z \quad (A.35b)$$

which indicates that the material behaves as though it were a fluid once it has reached its limiting shear resistance. Substituting Equation A.8 into Equation A.35a and considering the fact that $\dot{\epsilon}_{kk} = \dot{\epsilon}_z$, the vertical stress-strain increment relation in the plastic range becomes

$$\dot{\sigma}_z = K \dot{\epsilon}_z \quad (A.36)$$

Thus, the loading slope of the σ_z versus ϵ_z curve breaks or softens when yielding occurs and becomes equal to the bulk modulus. Accordingly, the loading slopes of the principal stress difference-pressure curve and the principal stress difference-strain difference curve become zero. The slope of the pressure-volumetric strain curve, however, is not affected and remains constant.

Once the material unloads, it behaves as a linear elastic solid again, satisfying Equations A.18 through A.25. If unloading is continued until the lower yield surface corresponding to

$$\frac{1}{\sqrt{3}} (\sigma_z - \sigma_y) = -k \quad (A.37)$$

is reached, the material flows plastically again and Equations A.8 and A.15 govern the behavior of the material.

The foregoing analyses are depicted schematically in Figure A.3. From Figure A.3 it can readily be seen that a Prandtl-Reuss material exhibits no hysteretic effects during a hydrostatic test. Furthermore, for a Prandtl-Reuss material, the vertical stress-strain curve from a uniaxial strain test would break or soften when yielding occurs and remain concave to the strain axis with continued application of vertical stress. These observations are generally contrary to existing experimental data on the stress-strain behavior of earth materials even from a qualitative point of view. This simply illustrates a fact of no great surprise, i.e. that the ideal linear elastic-plastic (Prandtl-Reuss) model does not adequately describe the stress-strain behavior of real, nonideal soils--in particular the behavior under conditions of uniaxial strain.

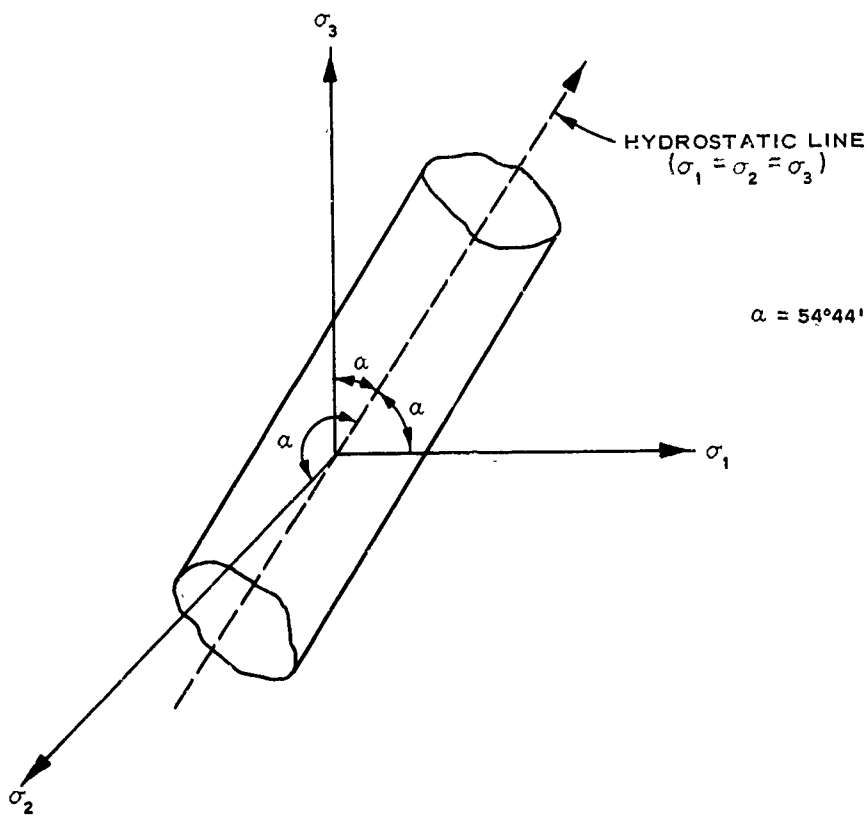


Figure A.1 von Mises yield surface in principal stress space.

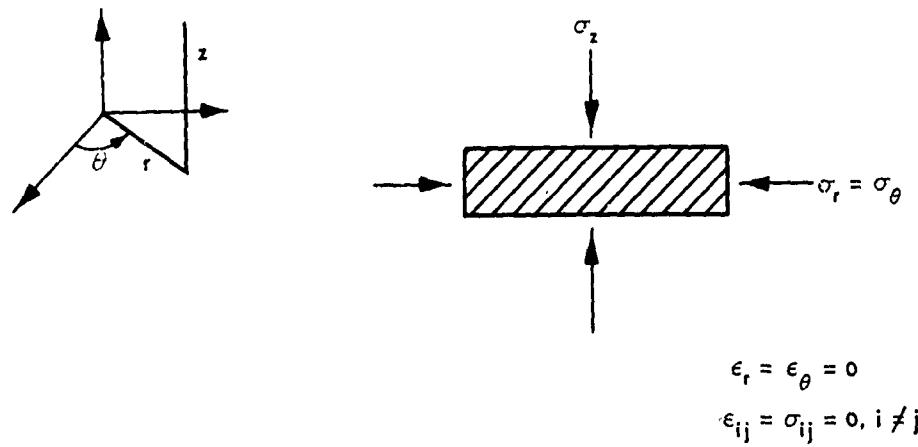
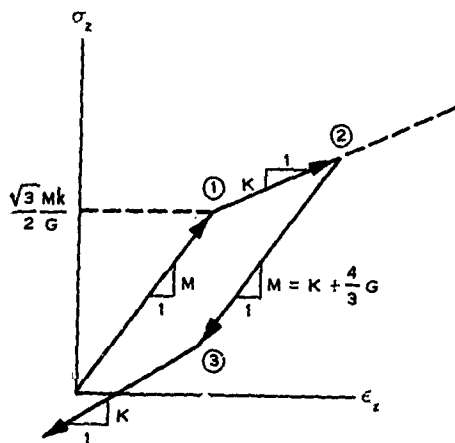
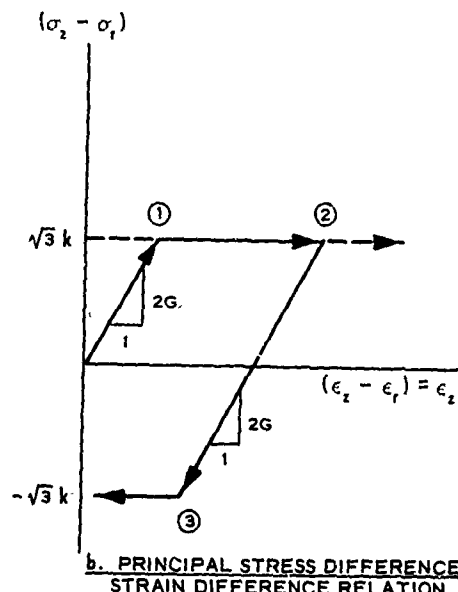


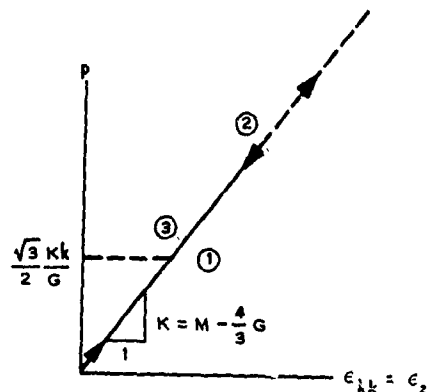
Figure A.2 Uniaxial strain configuration in cylindrical coordinate.



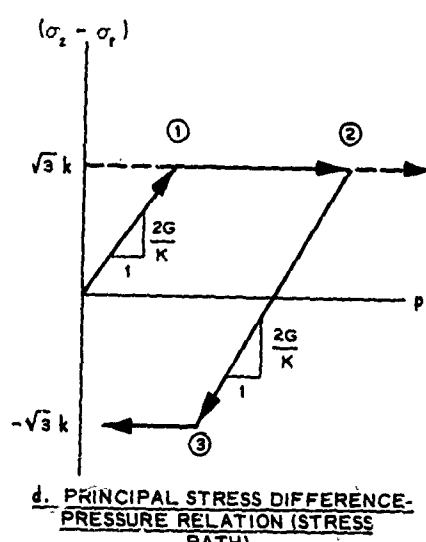
a. VERTICAL STRESS-STRAIN RELATION



b. PRINCIPAL STRESS DIFFERENCE-
STRAIN DIFFERENCE RELATION



c. PRESSURE-VOLUMETRIC
STRAIN RELATION



d. PRINCIPAL STRESS DIFFERENCE-
PRESSURE RELATION (STRESS
PATH)

Figure A.3 Behavior of Prandtl-Reuss material under conditions of uniaxial strain.

REFERENCES

1. I. Nelson and M. L. Baron; "Investigation of Ground Shock Effects in Nonlinear Hysteretic Media; Development of Mathematical Material Models"; Contract Report S-68-1, Report 1, March 1968; U. S. Army Engineer Waterways Experiment Station, CE, Vicksburg, Mississippi; prepared by Paul Weidlinger, New York, N. Y., under Contract No. DACA39-67-C-0048; Unclassified.
2. F. L. DiMaggio and I. Sandler; "Material Models for Soils"; DASA Report No. 2521, April 1970; Defense Atomic Support Agency, Washington, D. C.; prepared by Paul Weidlinger, New York, N. Y., under Contract No. DASA01-69-C-0130; Unclassified.
3. J. G. Jackson, Jr.; "Analysis of Laboratory Test Data to Derive Soil Constitutive Properties"; Miscellaneous Paper S-69-16, April 1969; U. S. Army Engineer Waterways Experiment Station, CE, Vicksburg, Mississippi; Unclassified.
4. E. Sternberg; "Nonlinear Theory of Elasticity with Small Deformations"; Transactions, American Society of Mechanical Engineers, March 1946, Vol. 68, Pages A53-A60; New York, N. Y.; Unclassified.